Fermi National Accelerator Laboratory

FERMILAB-Pub-87/182-E
[E-741/CDF]

Design and Construction of the CDF Central Tracking Chamber*

F. Bedeschi, J. P. Berge, J. Bofill, M. Dell'Orso, G. W. Foster,
M. Hrycyk, R. W. Kadel, J. Kowalski, A. Mukherjee, C. Newman-Holmes,
J. O'Meara, J. Patrick, D. Tinsley, R. L. Wagner, and R. Yarema
Fermi National Accelerator Laboratory
P.O. Box 500, Batavia, Illinois 60510

A. Byon
Purdue University
West Lafayette, Indiana 47907

A. Menzione, A. Scribano, A. Stefanini, and F. Zetti
I.N.F.N., University of Pisa, Pisa, Italy

July-August 1987

*Submitted to Nucl. Instrum. Methods A

DESIGN AND CONSTRUCTION OF THE CDF CENTRAL TRACKING CHAMBER

F. Bedeschi, J. P. Berge, J. Bofill, M. Dell'Orso, G. W. Foster, M. Hrycyk,
R. W. Kadel, J. Kowalski, A. Mukherjee, C. Newman-Holmes,
J. O'Meara, J. Patrick, D. Tinsley, R. L. Wagner, R. Yarema
Fermi National Accelerator Laboratory[1]

A. Byon
Purdue University

A. Menzione, A. Scribano, A. Stefanini, F. Zetti
INFN, University of Pisa, Pisa, Italy

May 8, 1987

Abstract

We describe the design and construction of a large drift chamber of a novel design well adapted for operation in high magnetic fields and in the high track density environment of hadron colliders.

1. Introduction

The Collider Detector at Fermilab (CDF) is a magnetic spectrometer surrounded by 4π electromagnetic and hadronic calorimeters. This report describes the design and construction of the Central Tracking Chamber (CTC) of the CDF detector which occupies most of the volume of the superconducting, solenoidal 1.5 T magnet, as shown in Fig. 1.

The goals of the CDF tracking systems are complementary to the calorimetry, in that the calorimetry tends to integrate over particles, whereas the tracking

[1] Universities Research Association under Contract with the U.S. Department of Energy No. DE-AC02-76CH03000

system provides information at the single particle level. The most important goal of the Central Tracking Chamber is to provide a measurement of the track parameters of isolated high P_t (transverse momentum) particles at both the trigger level and in the offline data reduction. This information, when combined with the calorimeter information, is critical to the identification of high momentum leptons, especially muons. The measurement of isolated high P_t particles can, however, be accomplished by much simpler tracking systems, and our design is largely dictated by two other physics considerations:

1. Measurement of high P_t particles in jet cores. Simulation studies show that lost or ambiguous information in high P_t tracks comes not from a background of crossing, low P_t particles, but from pairs (or more) of high P_t particles that stay close together throughout the tracking volume. This requires a design capable of identifying and separating two closely spaced tracks early in the pattern recognition process by incorporating internal data consistency checks via the chamber design.

2. Measurement of track parameters at angles below 30° with respect to the beam direction. This is difficult to do in a short solenoidal magnet, but the more layers at small radius (i.e. small angles), the better the measurement will be.

Other goals of the central tracking system include:

1. Identification of energy directed at cracks or holes in the calorimetry. This is needed for the analysis of events with large missing transverse energy (E_t).

2. Identification and measurement of secondary vertices coming from the decay of long lived particles. This requires a precision vertex detector close to the interaction region, but good, high precision track information from the CTC is essential.

3. Matching of tracks with shower centroids measured in the calorimetry. This is particularly useful in removing background from charged and neutral pions from electron candidates. This requires the ability to extrapolate tracks in three dimensions with a resolution of the order of a few millimeters.

4. Measurement of the charged particle transverse momenta and multiplicity as a function of rapidity and of the center of mass energy. We expect about 4 charged particles per unit rapidity in the central region.

5. Studying the response of the calorimeters as a function of momentum and position in the calorimeter.

The design of the CTC is also influenced by the specific environment of the CDF detector and at the Fermilab Collider. These include:

1. An interaction rate of 50,000 events per second at the design luminosity of $10^{30}\,\mathrm{cm}^{-2}\,\mathrm{sec}^{-1}$ dictates that the maximum drift time should be less than the beam-beam crossing time of 3.5 μ seconds.

2. The field of the CDF magnet is 15 kilogauss.

3. The interaction region is 1 meter long (FWHM).

4. The CTC is buried inside the detector and therefore reliability (e.g. redundancy, low power consumption, remote calibration) is important.

With these physics goals and environmental issues in mind, we have designed a tracking chamber with large drift cells arranged into superlayers. Each cell has multiple sense wires, and every wire is equipped with multi-hit electronics. Dividing the tracking volume into drift cells limits the total drift time and also permits a large number of measurements per track at reasonable cost. The use of multiple sense wires in a single cell allows ambiguous or corrupted information to be identified early in the analysis by looking at the correlated information between neighboring sense wires. Arranging the cells into superlayers permits the natural interleaving of cells providing r-ϕ information with stereo layers providing information about the r-z view. The long interaction region requires a chamber as long as the magnet permits and reducing everywhere the material between the chamber and interaction region. Reliability is enhanced by adding as much redundancy as is practical and economically possible.

We discuss the reasoning that led to this specific implementation. In the presence of crossed magnetic and electric fields electrons drifting in a gas move at an angle β with respect to the electric field direction given approximately by:

$$\tan \beta = \frac{\mathrm{v(E, B = 0)\, B}}{\mathrm{kE}}$$

where v(E,B=0) is the drift velocity (m/sec) without a magnetic field, E is the electric field strength (in V/m) and B is the magnetic field strength (in Tesla). The choice of a particular drift gas fixes the drift velocity (v) and the parameter (k). The parameter k is approximately 1 at low electric fields but decreases to $\sim$ .7

in Argon/Ethane/Ethanol (49.6%/49.6%/0.8%; our preferred gas) at the electric field relevant to CTC operation [Ref. 1]. With the design magnetic field of 15 KG and a desire to operate the chamber with an electric field as low as possible, yet sufficiently high so that the electron drift velocity in the gas of choice is saturated, a large value of the Lorentz angle β is indicated. In order to reduce dead space and linearize the time-to-distance relationship at the end of the cells caused by a large Lorentz angle, we can tilt the cells (and thus the drift electric field) with respect to the radial direction, so that in the presence of a 10 kG to 15 kG magnetic field the drift trajectories are approximately azimuthal. The drift angle may be varied within limits by choosing the electric field E, as long as E remains high enough that v remains saturated (i.e. $v(E) \sim$ constant).

There are advantages in making the tilt angle large. With the cells tilted at an angle with respect to the radius vector, the sense wire plane of each cell subtends a finite angle in azimuth from the beam axis. If the number of sense wires in the cell, the number of cells in a layer, and the cell tilt angle are all sufficiently large the cells can overlap each other. This guarantees that every radial (i.e. high P_t) track must pass close to at least one sense wire in every superlayer, a fact that is exploited in the trigger [Ref. 2]. This "zero crossing" condition on the drift times may be further exploited to help resolve closely spaced tracks. For tracks originating at the beam axis with P_t more than a few hundred MeV/c, the pattern recognition problem of resolving the right-left ambiguity is greatly simplified. This ambiguity is easily resolved because the ghost track defined by the improper assignment is rotated with respect to the true track direction by an angle $\Delta = \tan^{-1}(2\tan\beta)$

(approximately 70° in our case). Notice also that every radial track samples the whole range of drift distances in the cell, a fact used in the offline calibration of the chamber.

Our design has axial wire superlayers interleaved with stereo wire superlayers. Cells in the stereo layers are canted at $\pm 3^{o}$ with respect to the beam axis. The bulk of the pattern recognition is done using the axial layer data. This implies that it is desirable to have a large number of sense wire layers in the r-ϕ view. On the other hand, we want sufficient stereo data distributed at a variety of radii to allow good reconstruction precision in the r-z plane. A further requirement is that the position information from the tracking should match the position resolution of the calorimetry. Stereo wires with a resolution of 3 to 4 mm meet this requirement and are less expensive to implement than charge division.

With the above considerations in mind, we have chosen a tilt angle of 45° and large overlapping axial cells in layers interleaved with shorter stereo superlayers that provide r-z information. We summarize the performance specification for the CTC in Table I.

2. Overview

The central tracking chamber is a wire chamber with 84 layers of sense wires arranged into 9 superlayers. Five of the superlayers, in which the wires are parallel to the beam line, each contain 12 sense wire layers. These five axial layers are interleaved with four superlayers of stereo wires in which the angle between the sense wires and the beam line alternates between $\pm 3^{o}$. Each stereo superlayer contains 6 sense wire layers. Both axial and stereo superlayers are divided into cells

so that the maximum drift distance is less than 40 mm, corresponding to about 800 nsec of drift time.

The number of cells in each superlayer was chosen using several criteria: First, the aspect ratio in the axial superlayers was chosen so as to provide a significant azimuthal overlap (about 20%). Secondly, the cell size was chosen to be as large as possible to minimize the number of wires in the chamber, yet small enough to allow for convenient construction. With our choice, the average drift distance ($r\,\Delta\phi$) at the lower edge of the cell is about 35 mm. Thirdly, the number of cells was chosen to provide approximately equal drift distances in all superlayers. Finally, the number of cells in each of the superlayers was chosen to be divisible by 6, providing an exact hexagonal symmetry of the end walls. This was planned to aid in the construction and subsequent survey of the chamber.

Fig. 2a shows the cell configuration for the innermost axial layer. The direction of the electric field is approximately 45° with respect to the radial direction, and the drift direction is parallel to the phi or circumferential direction when the magnetic field is 15 kG, as shown in Fig. 3. Table II summarizes some of the mechanical properties of the chamber.

The resolution of a stereo wire in the longitudinal (z) coordinate, is expected to be approximately $0.2\,\mathrm{mm}/\sin 3^\circ = 4$ mm, equal to the position resolution of the calorimetry. Several additional layers of limited streamer drift tubes [Ref. 3] just inside the coil will provide a 3-dimensional space point for particles in the range of polar angles between 45° and 135° with respect to the beam direction. The longitudinal position resolution of these tubes should be 0.1% of the wire length or

about 3mm.

Each sense wire is connected to a multiple hit TDC, with the option available to add analog information (i.e. FADC's) at a later date. The double track resolution is expected to be less than or equal to 5 mm or 100 nsec. Cancellation of the 1/t tail of sense wire pulses due to ion motion (up to 250 nsec long) is accomplished by special filters in the electronics.

3. Electrostatics and Cell Configuration

Fig. 2b is a schematic diagram showing the placement of the wires in the chamber for one cell in the innermost axial layer. The boundaries of the cell are defined by two planes of field wires. In the case of axial cells, there are 31 wires in the field plane. The sense wire plane lies midway between the two field wire planes and contains 12 (6) sense wires for each axial (stereo) cell. Separating each sense wire from its neighbor is a potential wire which is used to control the gas gain on the sense wires, while the field wire voltages control the strength of the drift field. For our preferred gas, the Lorentz angle is 45° for electric fields of 1350 V/cm at magnetic fields of 15 kG. Because the cell is tipped, the electric field becomes very non-uniform at the extreme ends of the cell. Three special classes of wires have been added to keep the electric field uniform over the fiducial volume of the cell. These three classes of wires are: field plane guard wires, consisting of the first and last three wires in the field wire plane; sense plane guard wires, consisting of the first three and last three wires in the sense wire plane; and shaper wires, four wires per cell used to close off the top and bottom of the drift region. This nomenclature is displayed in Fig. 2b and will be used throughout the text.

The relative location of the sense and field wire planes and the voltages on the wires are adjusted so as to minimize the variation in the magnitude and direction of the drift field. It is worth noting that the location of the sense wire plane is not obtained by a simple rotation of a neighboring field wire plane. Rather, the optimal position for the sense wire plane can be shown to lie along a line connecting the midpoints of the two line segments joining the ends of the field wire planes (See Fig. 2c). The middle wire of the sense wire plane is chosen to lie at the midpoint between the two middle wires of the field wire planes. In this particular configuration, the electric field on both sides of the sense wire plane can be made equal by a simple linear grading of the voltages on the field wire planes. For economic reasons the wire-to-wire spacing on the sense wire plane is chosen to be the same as in the field wire plane (5 mm). This allows us to use the same hardware for the sense wire and field wire planes.

The "inside" cylindrical surface of the chamber at the inner diameter is covered with 0.003 in. (1.58 mm) thick copper clad Kapton and insulated from the aluminum frame of the chamber by an additional layer of Kapton. The interior surface at the outer diameter is covered by 1/16 in. thick copper clad G-10. These electrodes are operated at a potential of about -2 kV in order to prevent deterioration of the performance of the chamber near these surfaces.

We have made calculations of the electrostatic properties of our chamber design, requiring equal induced charges and minimal forces on all sense wires, and a constant electric field (both magnitude and direction) in the drift region. We have developed a computer program that allows us to calculate for an arbitrary

wire geometry the charges induced on each of the wires when a set of arbitrary potentials is applied to these wires, and thus to predict the electrostatic properties of our design. We use this program to perform a least squares adjustment of the set of applied potentials to yield optimal electrostatic properties for a cell of each of our superlayers. Our three fit criteria are: 1) the variation of charges induced as the sense wires around the desired value should be minimal; 2) the magnitude and direction of the electric field should be such as to yield the desired drift direction and velocity throughout most of the sensitive cell volume; 3) and that the electrostatic forces on the sense wires should be minimal. We have verified our predictions with measurements on prototypes, and in fact operate the CTC largely in accordance with these predictions. Here we summarize the findings:

1. The charges induced on all sense wires are made equal to better than 0.2%, ensuring adequate gain balance.

2. The drift field throughout the fiducial volume of the cell is kept constant to 1.5% rms, except near a wire plane.

3. The residual electrostatic forces on all sense wires are smaller than the gravitational forces, and only significant for the outermost sense wire in each cell.

With the geometry specified and assuming a resolution of 200 μm per point, we have calculated the measurement precision of the helix parameters of a track coming from the beam axis as a function of the layer to which it has penetrated. The results of this calculation are summarized in Fig. 4 (a-d).

4. Mechanical Considerations

The Central Tracking Chamber is a right cylinder of diameter 2760.0 mm and length 3201.3 mm (including the thickness of the endplates). Figs. 5 and 6 show the end and side views of the chamber, respectively. Each endplate is fabricated from 2.00 inch thick 6061-T651 aluminum. About 30% of the aluminum is removed to allow passage of the wires and insulators through the endplates. The inner free diameter of the chamber is 554.0 mm. The inner support cylinder is made from 2.0 mm thick Carbon Fiber Reinforced Plastic (CFRP) and supports an axial compressive load of 9.0 tons. Straightness and roundness of the inner cylinder are measured to be within 0.5 mm. This cylinder acts as the mechanical support and part of the gas seal for the vertex time projection chambers [Ref. 4] (VTPC, see Fig. 1). The total amount of material between the chamber and the beam is shown in Fig. 7.

The outer can of the tracking chamber is fabricated from 0.250 in. (6.35 mm) thick aluminum. As shown in Fig. 7, the outer can consists of a relatively open cage that is closed by eight hatch covers. Each hatch opening is approximately 0.84 m wide by 2.56 m long. The endplates of the CTC serve as the mechanical support for an array of approximately 2000 limited streamer drift tubes (CDT) located in the annular region between the drift chamber and the inner wall of the cryostat. (Fig. 1).

The choice of wire diameters and materials follows traditional thinking. Sense wires are made of 40 μm gold plated tungsten wire. All other wires in the chamber are made of stainless steel 304 wire with approximately 90,000 psi yield,

150,000 psi ultimate tensile strength, and 20% elongation. Stainless steel wire was chosen because it has a high work function (about 4.5 eV). The yield properties of the wire are necessary in the event of wire replacement, a process which involves stretching a wire approximately 5 cm. Diameters of the field and shaper wires in the chamber are graded to reduce the absolute value of the electric field on these wires.

Copper beryllium wire would be a more common choice for field wires because it is easier to solder. Unfortunately, it has a low work function and and must be silver or gold plated, which can reduce the surface quality, especially when one considers that there are over 150,000 meters of wire in the chamber.

Fig. 8 shows the shape of the endplate under the wire load. The deflection at the mid radius of the endplate is approximately 1.4 mm. The calculation assumed infinitely stiff supports at the inner and outer radius of the end plate. In fact, the outer compresses about 0.075 mm (smaller than the endplate flatness tolerance of 0.5 mm), while the inner support cylinder compresses about 1.0 mm. This has no effect upon the location of the axial wires, but stereo wires are displaced in an axially symmetric way up to 0.1 mm in the phi direction at the chamber endplates.

4.1 *Wire Mounting Scheme.* Four inches at each end of the chamber are reserved for wire mounting, electronics, cables and gas manifolds. Fig. 9(a,b) shows a cross section and side view of the wire mounting blocks used to hold and locate the wires on the CTC endplates. With the exception of shaper wires (see Fig. 2b), all wires are held in mounting blocks. Two kinds of wire mounting block are required for the CTC, one for stereo layers and one for axial layers. The two

types of wire block differ only in length: there are 31 wires in an axial block while a stereo mounting block contains 19 wires. The wire to wire spacing in the plane of the wires is 5 mm. The free, unsupported length of the wires from the east to the west endplate is 3214.0 mm, without correcting for the deflection of the endplates.

Each wire is held by a 0.040 in. (1.02 mm) (outside diameter) by 1.3 in. (33 cm) long crimp tube. The inside diameter of the crimp tube varies depending on the wire diameter; typically it is 0.003 in. (0.075 mm) larger than the wire diameter. The exception is the DHP copper crimp tube for the tungsten sense wires, which has an inner diameter of 0.016 in. (0.406 mm). The crimp tube for the stainless steel wire is fully annealed SS-304. The part of the wire block which supports the wire tension (via the crimp tube) is constructed of injection molded RYTON R-4 glass (Phillips Chemical Co.) reinforced plastic. The wire is located within the wire block by a precision machined 0.250 in. (6.35 mm) diameter fiberglass-epoxy "pulltrusion" rod glued into the RYTON block. Each wire rests in a groove with a 60° opening angle in the rod. The longitudinal location of the groove from the datum end of the rod is held to 0.012 mm, and the depth is controlled to account for the differences in wire diameters. The rods were measured to be straight to within $\pm$0.012 mm; additionally, the depth of every groove in the rods were measured and rods not meeting the tolerance criteria of $\pm$ 0.012 mm were discarded.

A great deal of attention was paid to reduce machining costs by making the endplates as low precision as possible. Most features on the endplate are machined with a tolerance of 0.015 in. (0.380 mm) ("true position", ANSI 14.5Y Standard). A set of 12 survey holes equally spaced on the perimeter of the chamber and a precision

surface on the i.d. of the chamber are the only features machined to high tolerance (0.0003 in. (0.008 mm) true position). The wire blocks are then positioned above "clearance holes" in the endplate by a special fixture that was referenced from the precision holes and surfaces listed above. This fixture, shown in Fig. 10, consists of a radial arm mounted on a pivot at the center of the chamber. The phi location of this arm is determined by a stop plate which is pinned during construction to 2 of 12 precision machined survey holes near the outer diameter of the endplate. The radial location of the wire block is then determined by a set of precision machined holes in the arm. Because of the six fold symmetry of the chamber, center locations of all of the 2640 wire blocks on both endplates can be reduced to a set of 140 locations (arranged in 5 rows) in the stop plate and 18 locations on the arm. These holes are machined to a tolerance of 0.0003 in. (0.008 mm) As each wire block was located on the endplate, it was first "tacked" in place with Eastman 910 glue, then screwed to the endplate, and finally reglued using 3M Structural Epoxy. The perimeter of each wire block was also glued to the endplate with Structural Epoxy to afford a gas seal and improve the mechanical stability. About 120 blocks could be installed in an eight hour shift. Due to the high thermal expansion coefficient of aluminum, this work was performed in a temperature controlled clean room, held at 20°C $\pm$ 1°C.

The wires of each mounting block pass through a slot machined in the endplates. In the case of the axial layers, the slot is 0.420 in. (10.67 mm) wide. Slots for the stereo layers are 0.420 in. (10.67 mm) wide at the outside of each endplate but the sides of the slot are tapered by 3° to allow more clearance for the stereo wires.

The wires are insulated from the aluminum walls of the slot by a DELRIN-500 (DuPont Co.) skirt, 1 to 2 mm thick depending on the type of cell.

Each shaper wire is held in a individual feed-through passing through a 0.130 in. (3.30 mm) ID hole in the end plate. The design of this feed-through is shown in Fig. 11. The wire is insulated from the aluminum endplate by high density polyethylene tubing. To reduce the value of the electric field on the surface of the dielectric, the 0.040 in. (1.02 mm) diameter crimp tube passes completely through the aluminum. The wire and crimp tube are swaged to an additional stainless steel sleeve supported on the outside surface of the endplate by a bushing made from NORYL EN265 (General Electric Co.) plastic. NORYL was chosen because of its good electrical properties (particularly surface conductivity) and mechanical strength.

After the wire blocks and insulating skirts are mounted on the endplates, the locations of four sense wire grooves per block were surveyed with an r-ϕ measuring engine employing a linear and an angular encoder readout via a CAMAC interface. The angular encoder is an Heidenhahn ROD-800 with an absolute angular accuracy equivalent to 0.012 mm at 2 meters. The linear encoder used to measure the radial coordinate is a Bausch and Lomb Acurite model AR-1, with an absolute accuracy of 0.002 mm over 2 meters. The angular encoder is mounted at the center of the endplate and the linear encoder is mounted to an arm which pivots about the axis of the angular encoder. A television camera, mounted on precision rails bolted to the radial arm, was used to locate the bottom of the v groove in the wires. Because the encoders are independent from the screw shaft that drives the camera location, the

survey is immune to errors caused by backlash. The magnification of the camera is about a factor of 60, and in small scale tests the measurement reproducibility was 0.005 mm rms in both coordinates. Fig. 12 shows the deviations of the measured positions from their theoretical locations. The width of the distribution indicates that the the wire locations within a superlayer should be accurate to 0.025 mm rms. Once the wire blocks were mounted and surveyed on both endplates, the entire outside surface of the endplates was potted in 3-M Structural epoxy to prevent gas leaks.

The endplates were then assembled vertically with the inner support tube and the outer cage assembly, using a system of plumb bobs hung via 100 μm diameter wires to align the two endplates rotationally and translationally. The locations of the plumb bob wires were monitored with respect to specially designed targets viewed via high magnification television cameras. The position resolution of this system allowed the endplates to be aligned to $\pm 25\,\mu$m. The axial distance between endplates was measured with a stick micrometer and held to $\pm 300\,\mu$m around the perimeter of the chamber. Four of the eight hatch covers were also glued into place in this configuration to maintain the orientation of the endplates during pretensioning. Subsequent surveys of the alignment of the chamber after wire-stringing indicate that the endplates were held in their theoretical positions to better than the 50 μm systematic error of the optical survey.

4.2 *Wire Stringing.* While the endplates are relatively thick, they do bend over 1 mm axially due to the combined tension of all the wires (25 tons). If this deflection is not properly taken into account, the wires in the chamber can go slack

or break. This problem was solved in our case by pretensioning the chamber with a system of about 1000 pretension wires, consisting of a length of 0.040 in. (1.02 mm) piano wire fixed on one end of the chamber with a bracket and held under tension on the other end by a helical compression spring with a spring constant of 30 lbs/in. (52.5 nt/cm). Approximately one pretension assembly per wire block was installed to deflect the endplates to their final shape prior to stringing. Each pretension wire carried a load of about 50 lbs. (222 nt).

The pre-stringing of the chamber began by installing the pretension wires and shaper wires under very low tension, starting at the innermost radius and working radially out. Along with each pretension wire, five (three) mylar strips per axial (stereo) wire block were inserted to act as a "feed" line to pull the real chamber wires through the chamber. After all pretension wires, shaper wires and mylar strips had been installed (with low tension), the remaining four hatch covers were mounted on the chamber. This procedure was chosen in order to preserve the alignment of the chamber: The net torque produced by the stereo layers under full tension is sufficient to twist the chamber by 0.5 mm at the outer radius if unopposed by the outer skin; and by 0.0075 mm with the outer skin in place. (The inner CFRP cylinder is rather weak in torsion, due to the unfavorable ratio of lever arms). By mounting the outer skin prior to applying the pretension, we successfully maintained the alignment of the chamber. In a similar vein, no welding was performed on the chamber during assembly: It is completely glued and screwed together.

The pretension was applied to the chamber starting at both the inner and outer radius and working towards the middle. The tension in the springs was

measured by compressing them to a known length. The springs compressed in the first stages were intentionally overcompressed so that as the full pretension was applied they would relax to their theoretical values. The first cycle brought the chamber to within 3% of the final load; a second iteration was performed to bring the pretension to its final value. The entire operation of installing the pretension wires, shaper wires, mylar strips, hatch covers and applying the pretension took about 5 weeks.

After pretensioning, wiring began by stringing those wires closest to the beam line first. Two crews worked on both ends of a horizontal diameter. In order to string the wires in a particular wire block, first the load on the pretension wire in that block was released. Each mylar strip was then used to pull a set of 6 or 7 wires into the chamber. The individual chamber wires were then tensioned using a set of standard weights strung over a low-friction pulley and crimped into place. An experienced crew of three technicians could string about 400 to 500 wires in an eight hour shift. The wire stringing was done during two shifts a day and the third 8 hour shift was used for measuring wire tensions and replacing wires with improper tension. Fig. 13 is a picture of the chamber about midway through the stringing process.

Wire tensions were measured [Ref. 5] by applying an "carrier" signal (3 Mhz) combined with a "resonant" (20-40 Hz) signal that swept through the mechanical resonant frequency of the wire under test. A mechanical resonance was induced by the interaction of the "resonant" signal current in the wire with a low magnetic field (800 amp-turns) generated by a coil that encircled half the chamber. The

resonance of this wire was monitored by using a neighboring wire to pick up the "carrier" signal radiating from the wire under test. The motion of the wire under test would modulate the carrier signal, with the maximum modulation occuring at resonance. An entire wire block was tested at one time under the control of an IBM PC, which automatically selected the wire, measured its resistance, tested whether it was crossed with neighboring wires and measured the resonant frequency. Sense wire tensions were held to 5% and field wire tensions to 10%, corresponding to location errors (due to gravitational sag) of $\pm 12\,\mu$m and $\pm 60\,\mu$m, respectively. Wires out of tolerance were replaced. About three and one-half months were required to string the chamber.

After the completion of the production stringing, the tension of all the sense wires were remeasured, and loose wires were replaced. Fig. 14 shows the resonant frequency distribution of all of the sense wires in the chamber. Following this operation, high voltage was applied to all the wires blocks in air to test for hot or noisy field wires, and any hot wires discovered in this operation were replaced. Due to humidity problems we could not test for noisy sense wires. This post-stringing process took about five weeks.

Thereafter the chamber was made gas tight. Clear plastic covers were glued over each wire mounting block to provide a gas seal. These covers also contain the high voltage busses and resistor chains used to apply the correct voltage to each wire. Hence, most of the voltage distribution is done inside the chamber gas volume, in order to avoid variations in leakage currents caused by humidity. Special, low insertion force contacts were used to make the electrical connection to the crimp

tubes. Shaper wire feed-throughs were sealed in an analogous manner.

4.3 *High Voltage System.* Every superlayer in the chamber requires 11 different high voltages for proper operation, corresponding to the 11 different "classes" of wires shown in Fig. 2b: inner and outer field plane guard wires (2), inner and outer field chain voltages (2), inner and outer sense plane guard wires (2), shaper wire voltages (4), and sense wire voltage. Twenty-seven of the 31 wires in each field wire plane obtain their voltages through a resistor divider mounted inside each field wire block (i.e. inside the gas volume). For the nine superlayers there are then a total of 99 different high voltage supplies plus one each for the inner and outer cylinder electrodes. In fact, we use 120 high voltage supplies as we connect no more than about 350 sense wires to a single HV supply in order to limit the total capacitance and thereby reduce the probability wires of breaking in case of a discharge. Since the chamber was made gas tight, no wires have broken.

To improve the redundancy of the system, each superlayer is divided into quadrants that can be turned on, off or grounded from the counting room via a mechanical switch box. This box also contains crowbar relays for dumping the stored energy contained in the power supplies, high voltage cables and chamber capacitance into an external resistor in about 10 msec.

The high voltage supplies themselves were specifically designed for the CTC, and we only discuss a few general features of the high voltage system here. The required voltage range is from 150 to 5000 volts, and the required current sensitivity is from 10 na (sense wires) to 1 ma (field plane resistor dividers). The chamber capacitance per supply ranges from 10 nf to 1 μf. Each supply has a programmable

voltage setting, programmable fast current trip, trip on power and a front panel overvoltage protection trip. The current readback is logarithmic with a sensitivity of 10 na or 1% of the current, whichever is greater. The 120 supplies are completely controlled by an IBM PC that ramps all the supplies on equally, in proportion to their final value. The software provides for individual software current trips (typically 50 times less than the programmable hardware fast trip); ramping (up and down) of individual channels, superlayers or the entire chamber; strip chart displays of up to 16 individual channel voltages and currents; a triggerable fast time display (1 msec per point) for examining current spikes; and an autoreset capability.

Each supply is fanned out in the switch boxes to four 70 m RG 58 cables that connect to resistive filter boxes mounted on the magnet yoke. These filter boxes protect the chamber from pickup on the HV cables and are used to equalize the decay time of the voltages in the chamber during a trip. The chamber is connected to the filter boxes via a miniature high voltage cable manufactured to our specifications by New England Electric Wire Co. Miniature cable was required due to space limitations. Each of the eleven voltage taps in a cell is connected to this HV cable via a "daisy chain" that includes blocking resistors to prevent cross talk between cells. These daisy chains were made from unshielded test lead cable with the blocking resistor and connector potted in 3M-DP110 epoxy, forming a "tee"; one "tee" per wire block in the daisy chain. We found in prototype tests that discharges due to static charge build up on the outside of the test lead cable caused noise in the chamber. This problem was solved by painting the outer surface of the

daisy chain with Eccocoat CC-40A conductive coating. After painting, each daisy chain was baked in an oven at 120° C for about 24 hours to reduce "dark" currents and then tested at 6000 volts for discharge problems. About 100 of the 7000 "tees" had to be rebuilt due to mechanical damage to the tees during installation on the chamber.

4.4 *Plumbing and Electrical Considerations.* The drift chamber gas is Argon/Ethane 50%/50% mixture bubbled through ethanol at $-7°$ C, corresponding to about 0.8% alcohol in the output stream by volume. The typical flow rate is $1\,m^3$/hr or one exchange of the chamber volume per day. The system, including the supply and return lines (2 in. i.d. (5 cm) stainless steel), is designed with a "fast flush" capability of $3\,m^3$/hr. The properties of the drift chamber are very sensitive to the alcohol concentration [Ref. 1] and several features of the gas system are intended to maintain a constant alcohol fraction. The input A/Ethane gas stream is precooled prior to the alcohol bubbler via a glycol/gas heat exchanger. At any given time there are about 4 liters of alcohol in the alcohol bubbler which is automatically refilled if the volume drops by more than 0.15 liters. Again, in order to maintain a uniform alcohol temperature, the "refill" alcohol is precooled prior to its introduction into the bubbler. The Argon/Ethane gas is introduced into the alcohol bath through 8 parallel $10\,\mu m$ stainless steel filters submerged near the bottom of the alcohol container. The alcohol temperature is kept constant to better than 0.1°C by submerging the container in a Neslab RTE-9DD bath refrigerator.

The 2 in. supply lines feed a manifold of twenty-five 3/8 in. (0.935 cm) tubes on the magnet yoke, each with its own electronic flow meter. Small diameter tubing

is used due to space limitations in the cable pathways between the endplug of the magnet and the end wall of the return yoke. These tubes are in turn connected to a distribution manifold mounted on the inside wall on the west end of the chamber. Identical plumbing on the east end is used to remove the gas. The output gas from the chamber is analyzed once a day for oxygen content (typically 20 ppm) and released to the atmosphere. Sample tubes on the outside of the chamber but inside the volume determined by the inner wall of the cryostat and the endplugs are used to monitor the ethane concentration inside this confined space. The oxygen concentration in this volume is maintained at about 1% by a nitrogen inerting system, in order to reduce the possibility of a fire caused by a catastrophic failure of the chamber gas seal or input manifold. The nitrogen flow in the inerting system is sufficient to dilute the ethane in the input stream to a level below the lower explosive limit (3.5% by volume) in air. Automatic systems are provided to shut down the HV system and low voltage systems and cut off the input gas in the event of a gas leak or fire. Without the nitrogen inerting system the chamber gas oxygen concentration is about 30 ppm.

Low voltage power and the chamber ground for the preamplifiers is provided via 9 circumferential circuit boards fastened to the outside of the endplates in the space between layers. These same circuit boards also act as the mechanical strain relief for the preamplifier cards, low and high voltage cable, and gas supply tubes. Each superlayer is divided into 4 sectors with separate high voltage, low voltage and calibration connections. Fig. 15(a,b) is a picture of the endplate of the chamber after installation of the preamplifiers.

The endplates on the two ends of the chamber are cooled by water circulating at the extreme outside and inside diameter (four cooling loops total). The outer copper cooling tube is glued to the chamber with thermally conducting epoxy, and the inner loops are soldered to the removable flange assembly that makes up the VTPC gas seal. About 4 liters of water per minute at 55°F are circulated in each cooling loop.

The cryostat of the superconducting magnet acts as a refrigerator on the outer skin of the chamber with a cooling capacity of about 500 watts. While some of the heat generated by the electronics is used to counter-balance this refrigeration, the relative locations of the heat sources and sinks are geographically isolated in a way that makes it difficult for them to cancel each other without causing large temperature variations. The outer surface of the drift tubes is therefore equipped with heaters to counterbalance the refrigeration of the coil. These heaters typically dissipate 135 watts into the tracking volume. The remaining heat necessary to cancel the cooling of the cryostat originates from the VTPC's and is transferred to the outer diameter of the CTC via convection through the drift chamber gas. About 100 thermal sensors are used to monitor the temperatures of the outer diameter, inner diameter and endplates of the CTC.

5. Electronics

Fig. 16 is a block diagram of the CTC data acquisition electronics for a single sense wire. Diagrams of the individual electronic components are displayed in Figs. 17, 18, 19, and 20. Each sense wire is connected to a preamplifier mounted directly on the chamber body. Miniature 56 ohm coaxial cables are used to transmit the

analog signals to an intermediate circuit which shapes the pulse, amplifies it and produces a time over threshold logic signal. This circuit, known as the Amplifier-Shaper-Discriminator, or ASD, is mounted on the magnet yoke, and provides an auxiliary analog output for each sense wire. The ASD discriminated signals (differential ECL) are fed to FASTBUS TDC's in the counting room via 70 m of flat cable. Trigger outputs for hardware processing are available as TTL outputs on the FASTBUS auxiliary connector.

5.1 *The Preamplifier Card*: The function of the preamplifier card (Fig. 17) is to provide fast, low noise amplification of the signals from the sense wires and to eliminate wire to wire cross talk caused by motion of positive ions. Specifications for the preamplifier are listed in Table III.

Sense wires are run at positive high voltage and are decoupled from the preamplifier circuit by a 1200 pF, 3KV blocking capacitor. The motion of positive ions away from an individual sense wire gives rise to a signal on neighboring wires with the same time dependence as the original sense wire signal but of opposite polarity and reduced magnitude (so-called "opposite sign cross talk"). In the case of the CTC, about 7% of the signal on a sense wire appears on the nearest neighbor and about 3% on the second nearest neighbor. This signal can be large enough to affect the timing of the real (versus cross talk) signals and must be corrected if optimum timing information is to be obtained. This is accomplished in our case by a passive resistor network which feeds part of the charge from a sense wire into the neighboring ± 2 wires. In actuality, we do not completely cancel the cross talk signal (about -1% remains) as a hedge against capacitive (or bipolar) crosstalk on

the preamplifier circuit board, cables or in the ASD cards. Putting the crosstalk network ahead of the preamplifier means that the cross talk is correctly cancelled independent of any electronics saturation. This is done at the expense of a slight increase the input noise. Each preamplifier is protected against chamber breakdown by a back to back diode pair and two current limiting resistors. The resistors are chosen so as to provide a series termination for the sense wire, when added to the input impedance of the preamplifier. The far end of each sense wire is also terminated to cancel reflections and a cross talk resistor connects neighboring sense wires to further reduce cross talk between wires.

The hybrid preamplifier (10354, Fig. 18) was designed by Velco Radeka of Brookhaven National Laboratory and manufactured for FNAL by Centralab of Wisconsin. The output signal for a minimum ionizing particle at 90° with respect to the beam line has a rise time of about 8 nsec (10% to 90%), an amplitude of about 40 mV and a RC decay time constant of approximately 40 nsec. The baseline to baseline width of a typical signal is 250 nsec. To reduce power consumption, the pull down resistor for the final emitter-follower is located outside the magnet on the ASD card. The cable between the preamplifier and ASD is 10 meters of miniature 56 ohm coaxial cable, electrically similar to RG174, and manufactured to our specifications by the New England Electric Wire Co. These output cables are packaged into a flat cable 1.3 mm thick and 34.2 m wide containing 26 cables, 24 for signals and two for calibration. Hence, two axial or four stereo preamplifier cards are read out on the same cable.

5.2 *The Amplifier-Shaper-Discriminator*: Fig. 19 is a block diagram of a single channel of the ASD circuit; Fig. 20 shows the details of the electronic design. Specifications for the ASD are given in Table IV. Power is provided to the final emitter follower of the preamplifier via the resistors R2 and R3. Resistor R4 terminates the coaxial cable. Transistor Q1 is an emitter follower to drive the pole zero filter consisting of R8, R9 and C6. The signal is then amplified by a factor of 20 using the NE592 video amplifier. The net voltage gain after the filter and NE592 is typically a factor of five. One quarter of a high speed comparator (U2 = LeCroy MVL407) is used as a discriminator on the output of the NE592 to produce a differential ECL pulse whose width is equal to the time over threshold of the input signal. The threshold is derived from the power supply voltages and is adjustable through a 100 to 1 voltage divider. Transistor Q2 and Q3 are differential drivers for the analog output. R17, R18, C13 and C14 are part of a cable compensation network which corrects for the dispersion of the cable between the ASD and the TDC, at the expense of a reduction in the output pulse height.

5.3 *FASTBUS TDC*: In order not to affect the resolution of the chamber, the TDC used must have a time resolution of better than 1 nsec, a range of about 1 μsec, and be capable of recording at least 8 hits per wire per event. To meet this specification we have chosen Lecroy 1879 FASTBUS TDC's. The TDC's are connected to the ASD's on the magnet yoke via 70 m of flat ribbon cable. Sixty-six TDC's arranged in 6 crates are used to readout the CTC.

The TDC's in each FASTBUS crate are read out by a modified version of the SLAC Scanner Processor (SSP) [Ref. 6], a general purpose FASTBUS master

device which emulates the IBM integer instruction set. The SSP in addition sorts the TDC data by wire number and time, and associates leading and trailing edge hits. The reformatted data from the SSP's is then read by the host VAX. In a typical $\bar{p}p$ event about 5500 words (1 word per hit) are read from the TDC's.

5.4 *Timing and Calibration.* Fig. 21 shows the general layout of the data acquisition and calibration systems. Shown in this figure are: the interconnections for a single channel of TDC readout; the interface between the CDF master clock system and the TDC system and a calibration card (cross hatched part of diagram) that decodes the information down-loaded from the data aquisition system and fans-out the calibration signals to the selected ASD cards or pre-amplifiers. Critical timing paths in this diagram are indicated by double lines. The total delays in these interconnections must be known in order to calibrate individual channels.

Four timing signals from the master clock system control the TDC system. They are: clear and strobe (C&S), beam crossing (B/C), pseudo beam crossing (PB/C), and beam gate/calibration gate (BG/CG). These timing signals are processed in the custom built gate generator to produce the clear and stop pulses needed by the TDC. They are fanned out to the individual TDC cards in a crate by a LeCroy 1810 Calibration and Timing (CAT) FASTBUS module, which drives these signals onto the FASTBUS backplane. The common stop is generated via a BNC 7075 delay generator. The calibration system uses a LeCroy 4222 programmable delay time generator, controlled via CAMAC to generate calibration signals at the preamplifier or ASD inputs.

5.5 *The Calibration Card.* The calibration card performs several functions. It enables a set of gates that route calibration signals to the desired preamplifier cards. A DAC on the calibration card is used to determine the charge injected into the pre-amplifiers. The calibration card contains an additional switch that allows a signal of fixed amplitude to be applied simultaneously to all the inputs of the 48 channels on an ASD card.

The timing of the calibration signal is kept separate from the analog (or pulse height) information by passing the timing signals through a system of gates and cables of known delay. The DAC on the calibration card is used to charge a calibrated capacitor at the input of each pre-amplifier channel to a pre-determined voltage. This capacitor is then discharged by an FET switch that is closed by the timed calibration signal, thereby injecting charge into the preamplifier.

There are five calibration channels per ASD card. Four of these channels are fed from the ASD card to the input of the four preamplifier cards per ASD card. Any combination of these four preamplifier cards may be selected. This feature was included to prevent degradation of the calibration information due to coherent effects passed through the power supply connections, etc. There is no provision for calibrating an individual channel on a pre-amplifier card independently of the other channels on that pre-amplifier card. In the case of stereo layers, each calibration channel is connected to two stereo pre-amplifier cards.

The fifth calibration signal per ASD card is connected to the inputs of the ASD. This feature is used for debugging the system and isolating whether a fault in the system is at the preamplifier (i.e. inside the solenoid) or at the ASD card

(on the magnet yoke). The charge injected into the ASD is not programmable, but corresponds to a minimum ionizing signal.

5.6 *The Calibration Sequence.* Calibration is initiated by a process in the host VAX. The user decides which channels are to be calibrated, the particular calibration test pulse to be used, either CAT, ASD or preamplifier, and the amplitude of the pulse to be input to the preamplifier. The host VAX downloads the first delay time into the programmable delay generator and the channel and pulse height information into the calibration modules. A number of events, typically 50, are taken. For these events, the SSP accumulates summary information including the average leading edge time and associated variance, the average pulse width, the number of TDC hits per event, and the fraction of events with data. This summary data is read from the SSP by the host VAX, and the process repeated for a number of different delay settings. When data from all delay settings has been read, a linear fit is made to the average observed TDC time versus delay setting for each channel, giving a slope and an offset time. These are compared to an expected range of values, and bad channels flagged. This information is recorded in a database and the offset information is then used by the offline reconstruction program to correct the raw TDC data prior to pattern recognition.

6. Initial Operation

The following is meant to describe in a cursory way the initial operation of the chamber and some of the more practical operational problems encountered. We expect to publish more complete results on our operating experience with the chamber and track reconstruction at a future date.

Prior to installation in the magnet, the chamber was tested for about two weeks in gas at high voltage. For the first 3 days of this period the chamber was flushed with pure Argon gas and burned in at about 50% of its normal operating voltage. Argon is a poor insulator and will initiate a nice glow discharge at modest voltages which is useful in cleaning up dirt and dust without a lot of stored energy in the chamber. Next, the chamber was flushed with Nitrogen and run slowly up over several days to near operating voltage (As we had not received the final high voltage system, we ran the chamber up to as high a voltage as was allowed by the number of power supplies available). About 20 hot wires, including 5 sense wires, were detected and replaced.

Finally, the chamber was tested in Argon/Ethane/Alcohol for three days. A typical chamber pulse is shown in Fig. 22. A handful of hot wires were located and replaced. Dark currents on the sense wires were typically 100 namp for 350 wires and the counting rates were consistent with cosmic rays (about 100 Hz per wire). The chamber was then moved to the CDF assembly hall, a four hour trip of about 500 yards.

Prior to the actual chamber installation, all of the FASTBUS system, ASD crates, cards, power supplies and cables had been installed on the detector or in the counting room and tested. The total time to install the chamber in the solenoid and connect the signal and HV cables was about five weeks, which includes the installation time for the VTPC and drift tube system.

The chamber was tested for two days in Argon/Ethane/Alcohol before the CDF detector was moved to the Collision Hall. During this period it was noted that

the chamber currents were typically 1 to 2 μa amps/350 wires and the counting rates were about 2 KHz per wire. For these tests the magnet was off. Initially this high rate was thought to be due to contamination of the gas, but subsequent tests suggests that the origin of the current is the 48 uranium bars used as absorber in the "Crack detectors" of the CDF Central Calorimetry. These uranium bars cover about 5% of the solid angle of the CTC and are located immediately outside the cryostat, separated from the CTC by the equivalent of 8 cm of aluminum. Our tests indicate that the current and rates in the chamber are consistent with radiation from the Uranium. The aluminum in the coil is sufficient to attenuate the rate by about 60%, and range studies indicate that the energy of the radiation is in the range 100 KeV to 1 MeV. One quarter inch of lead, which is about 6 mm thicker than the available space, has no effect on the rates or current. When the magnet is energized, the absolute rates on the wires drop to about 700 Hz, but a new class of pulses appear on the wires as shown in Fig. 22. These pulses are believed to come from low energy electrons which spiral in the 15 KG field and deposit their energy on a single wire. The bending radius for a 1 MeV/c electron is about 2 mm, consistent with the range studies mentioned above. The unusual shape of the pulses comes from the pole-zero filter in the ASD, which for pulses long with respect to 60 nsec acts as a voltage divider. As the energy deposited by these electrons is of order 100 times minimum ionizing, they tend to cause crosstalk in the chamber. The ballistic response of the amplifier is such that it continues to ring for up to 60 μsec after such a pulse. The rate of such saturating pulses is about 100 Hz per wire and independent of the beam intensity. It is planned to remove the uranium.

This high rate on the wires caused two sections of the chamber to go into "glow" mode. As access to the CTC was not possible for another month; these two quadrants (out of 36) eventually had to be shut down. Four other quadrants were shut down due to high voltage discharge problems between the daisy chains and chamber ground that only developed after the chamber was brought to full voltage with the final HV system. During the single access to the chamber during the run all but one quadrant of the chamber was made operational. The remaining bad quadrant had four adjacent supercells with many hot sense wires. These cells were strung during the same shift, and the problem is consistent with bad wire or improper stringing technique. Due to lack of time we decided not to replace these wires and run with this quadrant at reduced high voltage (approximately 1000 V below normal voltage on the field wires).

Until we gain more operating experience, high beam related currents in the chamber require that the inner layers of the chamber be operated at reduced voltages. The innermost layer operates at 94% of the design voltage and the typical current draw is 8 μa for the 360 wires in this layer at a luminosity of $6 \times 10^{28}\ cm^{-2}\ sec^{-1}$. The operating voltages gradually increase with the radius of the chamber such that by the fifth superlayer the chamber is being run at full voltage. Preliminary studies indicated that the wire efficiency of the chamber is greater than 98.3%, with most of the inefficiency coming from the inner layers.

Fig. 23 shows the reconstructed tracks and associated hits for a 2-jet event in the chamber. The right-left ambiguity in this particular display has not been removed from the raw data, producing a characteristic "X" pattern as a track

crosses through the sense wire plane. Points from stereo layers are plotted using the wire positions at the center of the chamber. The data has been corrected from the electronic calibration on a wire by wire basis. Fig. 24 shows a raw TDC distribution from superlayer zero. The distribution is characterized by a sharp rising edge, a long plateau from the linear drift region and a softer trailing edge because the outer wires in each superlayer have a longer maximum drift time than the inner wires. The average pulse width is 60 nsec, which corresponds to a 3 mm double track resolution.

Using a linear drift time relationship with the drift velocities scaled to account for the reduced voltages in the inner layers, the residual distribution for fitted tracks with momentum above 800 MeV/c and reconstructed in 3 dimensions is consistent with a gaussian distribution with a width of 220 μm. This distribution is shown in Fig. 26. If low momentum tracks are included, the distribution broadens to 250 μm. Work is now underway to extract drift constants information from the data; to reduce the sensitivity of the electronics to cross talk from large pulses; understand the double track resolution; and improve the pattern recognition and tracking efficiency. This will be the subject of a later paper.

7. Summary

We have described the construction of a large drift chamber for the CDF experiment at Fermilab. This chamber was designed to study interactions in a high track density environment and utilized the strong magnetic field of the CDF solenoid to its advantage, both in terms of pattern recognition and trigger capabilities. The chamber was three years in fabrication and is now taking data after a relatively

short break-in period. Ninety-five percent of the chamber was operational for this initial run.

8. Acknowledgements

The authors wish to point out that the concept of this design is not original with them but was first seen by one of them (RWK) in an early proposal for the ALEPH detector at LEP. We also wish to acknowledge the many frank discussions with our colleague's at SLAC, particularly Dr. Gail Hanson, who have built a chamber of similar design, although without tilted cells [Ref. 8]. We profitted greatly from their experiences.

Naturally, such a large project could not have been completed without the support of many technical and service personnel. The Fermilab Purchasing Department; Drafting Department, especially Chuck Grimm; shop; technical support personnel; our technicians Humberto Gonzalez, Lisa DesJardine, and Sara Gonzalez; and a large crew of very patient wire stringers, all did an outstanding job to help bring this project to a successful conclusion. To them we owe a debt of thanks. John Robb, Rich Krull and Roger Bossert were instrumental in installing the chamber and related cabling. We would also like to thank M. Ono (now at KEK) for his help during the early part of the project, and J. Huth for survey and calibration work.

Figure Captions

1. Cross section through a vertical plane of one half the CDF Detector. The detector is symmetric about the midplane and roughly symmetric around the beam axis.

2. a) Wire geometry for three super cells in the innermost 3 superlayers. Crosses indicate the sense wires. The radial direction at the center of the cell is in the direction of the arrow. Box surrounds the area magnified in Fig. 3b. Wire nomenclature for an axial cell. c) Schematic diagram of the cell geometry. Distances labeled by the same variable name have the same length.

3. Drift trajectories in a 15 kG magnetic field. The radial direction is indicated by the arrow.

4. a) Estimated momentum resolution of the CTC as a function of the layer penetrated. The three curves represent the resolution of the CTC for three different constraints on the impact parameter: no constraint, 100 μm and 1 μm. b) Estimated resolution of the impact parameter as a function of layer penetrated. c) Estimated measurement resolution of the dip angle for two different beam constraints. For tracks leaving the chamber between layers 12 and 30 there is still a sign ambiguity in the dip angle. d) Estimated measurement error in the longitudional (z) vertex coordinate as a function of the layer penetrated.

5. End view of the Central Tracking Chamber showing the location of the slots in the Aluminum endplates.

6. Side view of the Central Tracking Chamber. The outer cylindrical shell is made of 64 separate pieces of 1/4 in. thick aluminum glued and screwed together.

7. Total amount of material between the CTC and the beam as a function of

angle.

8. Deflection of the endplate as a function of the radial coordinate. The maximum deflection of the endplate is 0.048 in. (1.12 mm).

9. a) Cross section of the wire mounting block. b) Cut away view of a wire mounting block, indicating the relative locations of the pulltrusion rod and the holes for the crimp tubes.

10. (a) Top view of the locating fixture for the wire blocks showing the pivot at the center of the chamber, the radial arm and the stop plate fastened to two of the six survey holes. As shown the fixture is set up to locate a wire block in the outermost layer. b) Detail of the fixture used to locate the wire blocks. Outlines of both the axial and stereo blocks are shown at the bottom of the the figure. The plunger like device is the spring loaded fixture (with only vertical motion) used to capture the two ends of the pulltrusion protruding from either end of the wire mounting block. The round ends of the pulltrusion are located by the two v-blocks at the bottom of the plunger. The datum end of the pulltrusion rod (left hand side in the figure) is held against a stop by a spring loaded clip pushing on the opposite end (right hand side in the figure) of the pulltrusion rod.

11. Schematic diagram of a shaper wire feed-through.

12. Measured average deviation of the wire block locations as a function of the superlayer number. Data points are the average values and the error bars represent the rms of the distributions.

13. A picture of the CTC during wire stringing. Clealy visible are the mylar strips on the endplate used to pull the sense wires into the chamber. The air cooled coil used to generate a magnetic field for the wire tension measurements is seen in "park" position going vertically up over the top of the chamber. For measuring operations it was rotated down into a horizontal plane.

14. Mechanical resonant frequency distribution for all sense wires in the chamber. The curve is a gaussian distribution fit to the data of width 0.68 Hz corresponding to a 3% rms variation in wire tension. Of the remaining 8 wires, 6 were over flows and 2 wires were later restrung with 120 micron stainless wire due to mechanical interference problems that caused wires in these two locations to break.

15. a) The endplate of the chamber after installation of the pre amplifer cards and High Voltage daisy chains. The amplifer cards for the axial layers and the HV distribution for the stereo layers are mounted on this end of the chamber. b) Detail of several preamplier cards, showing the hybrid preamplifer chips.

16. Overview of the data acquisition system for a single wire. SSP is an accronym for Stanford Scanner Processor, a FASTBUS master with a mircoprocessor control, dual ported memory and connections to both the FASTBUS crate segment and a cable segment.

17. Circuit diagram for the preamplifier card.

18. Circuit diagram of the hybrid preamplifier. Circuit is formatted as a single in-line package.

19. Block diagram of the Amplifier-Shaper-Discriminator (ASD).

20. Circuit diagram for the ASD. Forty eight channels are packaged on a single 12 in. x 16 in. sized card using mostly surface mount technology.

21. Schematic diagram of the calibration network. Cross hatched area represents the circuitry contained in a calibration card in the ASD crate. Double lines indicate critrical timing paths that must be measured prior to calibration.

22. a) Typical pulse from the drift chamber during beam conditions. b) Saturating pulse from Compton electrons generated by gamma rays from the Uranium Crack detectors. The initial peak comes from the pole-zero filter in the ASD, which for times long with respect to 60 nec looks like a voltage divider. Note the change in vertical with respect to a) above. c) Detail showing the ringing of the Amplifer network after a saturating pulse. The chamber threshold is set to the equivalent of 35 mV on this scale.

23. A typical $\bar{p}p$ event in the chamber. Both the right and left drift ambiguities are shown in this particular display. Points on stereo tracks are plotted using the wire locations at the center of the chamber. The blow-up on the left corresponds to the box indicated in the main figure. The horizontal and vertical scales in this magnified view are distorted.

24. TDC distribution for one superlayer in the chamber. The hoizontal scale is in TDC counts.

25. Residual distribution for tracks reconstructed in 3 dimensions with a minimum

momentum of 800 MeV. The curve is a gaussian fit to the data with an rms width of 220 μm.

Table 1: Performance Specification

Gain:	3 x 10^4 (250 nsec gate)
Resolution:	$< 200\,\mu$m per wire
Efficiency:	$> .98$ per point
Double Track Resolution:	< 5 mm or 100 nsec
Maximum Drift Distance:	40 mm
Maximum Hits Per Wire:	> 7
Stereo Angle:	$\pm 3^\circ$
Z Resolution:	$< 0.200\,\mathrm{mm}/\sin 3^\circ) = 4$ mm
Momentum Resolution:	$dP_t/P_t < 0.001 * P_t$ (in GeV/c at 90°)

Table 2: Mechanical Parameters

Number of Layers:	84
Number of Superlayers:	9
Stereo Angle:	$0^\circ\ +3^\circ\ 0^\circ\ -3^\circ\ 0^\circ\ +3^\circ\ 0^\circ\ -3^\circ\ 0^\circ$
Number of Super Cells/Layer:	30, 42, 48, 60, 72, 84, 96, 108, 120
Number of Sense Wires/Cell:	12, 6, 12, 6, 12, 6, 12, 6, 12
Sense Wire Spacing:	10 mm in plane of wires
Tilt Angle (Center of Plane):	45°
Radius at Intermost Sense Wire:	309 mm
Radius at Outermost Sense Wire:	1320 mm
Wire Length:	3214.0 mm
Sense Wire Diameter/Tension:	40 μm gold plated Tungsten/135 g
Potential Wire Diameter/Tension:	140 μm Stainless Steel 304/661 g
Field Wire Diameter/Tension:	178 μm Stainless Steel 304/429 g
Guard Wire Diameter/Tension:	254 μm Stainless Steel 304/875 g
	305 μm Stainless Steel 304/1259 g
Shaper Wire Diameter/Tension:	305 μm Stainless Steel 304/1259 g
Total Number of Wires:	36,504
Total Wire Tension:	25 tons
Endplate:	2 in. Aluminium 6061-T6(51)
Outer Can:	0.250 in. Aluminum
Inner Support Cylinder:	0.080 in. Carbon Fiber Reinforced Plastic
Gas:	Argon-Ethane-Alcohol (49.6%::49.6%::0.8%)
Drift Field (E_o):	$\sim$1350 V/cm^2
Drift Field Uniformity:	dE_o/E_o $\sim$1.5% (rms)

Table 3: Preamplifier Specifications

Gain (Delta Function Input):	Vout = Qin/C ~ Qin/3 pf
Dynamic Range:	450 mV (1.5 pC)
Gain Uniformity:	~ 5% channel to channel
Noise:	~ 5000 electrons (100 nsec gate)
	source capacitance ~ 70 pF
Rise Time:	< 4 nsec
RC Decay:	~ 40 nsec
Power:	< 60 mW/channel
Cross Talk:	< 1% (overall system crosstalk)
Calibration Input:	One per card (selectable)
	< 1 nsec accuracy
	dynamic range 0.002 to 1.5 pC

Table 4: Amplifier-Shaper-Discriminator (ASD)

Voltage Gain:	$\sim$ 5 (after filters)
Output Width:	$<$ 90 nsec
Time Slewing:	$<$ 4 nsec (2x to 10x threshold)
Minimum Threshold:	$<$ 10 mV
Dynamic Range:	$\sim$ 2 V
Gain Uniformity:	$\sim$ 5% channel to channel
Cross Talk:	$<$ 1% (overall system crosstalk)
Analog Output:	Differential, 110 ohm
Discriminator Output:	Differential ECL, $\sim$ 110 ohm
Calibration Input:	One per card (selectable)
	$<$ 1 nsec accuracy

References

1. M. Atac et al., Nucl. Instrum. and Methods.

2. G. W. Foster et al., "A Fast Hardware Trigger Processor for the CDF Central Tracking Chamber." Submitted to Nucl. Instrum. and Methods.

3. S. Bhadra, "The CDF Central Drift Tube System," submitted to Nucl. Instrum. and Methods.

4. F. Snider, "The CDF Vertex Time Projection Chamber System," submitted to Nucl. Instrum. and Methods.

5. J. Bofill, "A computerized Electromagnetic Measurement of Wire Tension," to be submitted to Nucl. Instrum. Methods.

6. H. Brafman et al., IEEE Trans. NS32, 336 (1985).

7. G. Hansen, Nucl. Instrum. and Methods A252, 343 (1986).

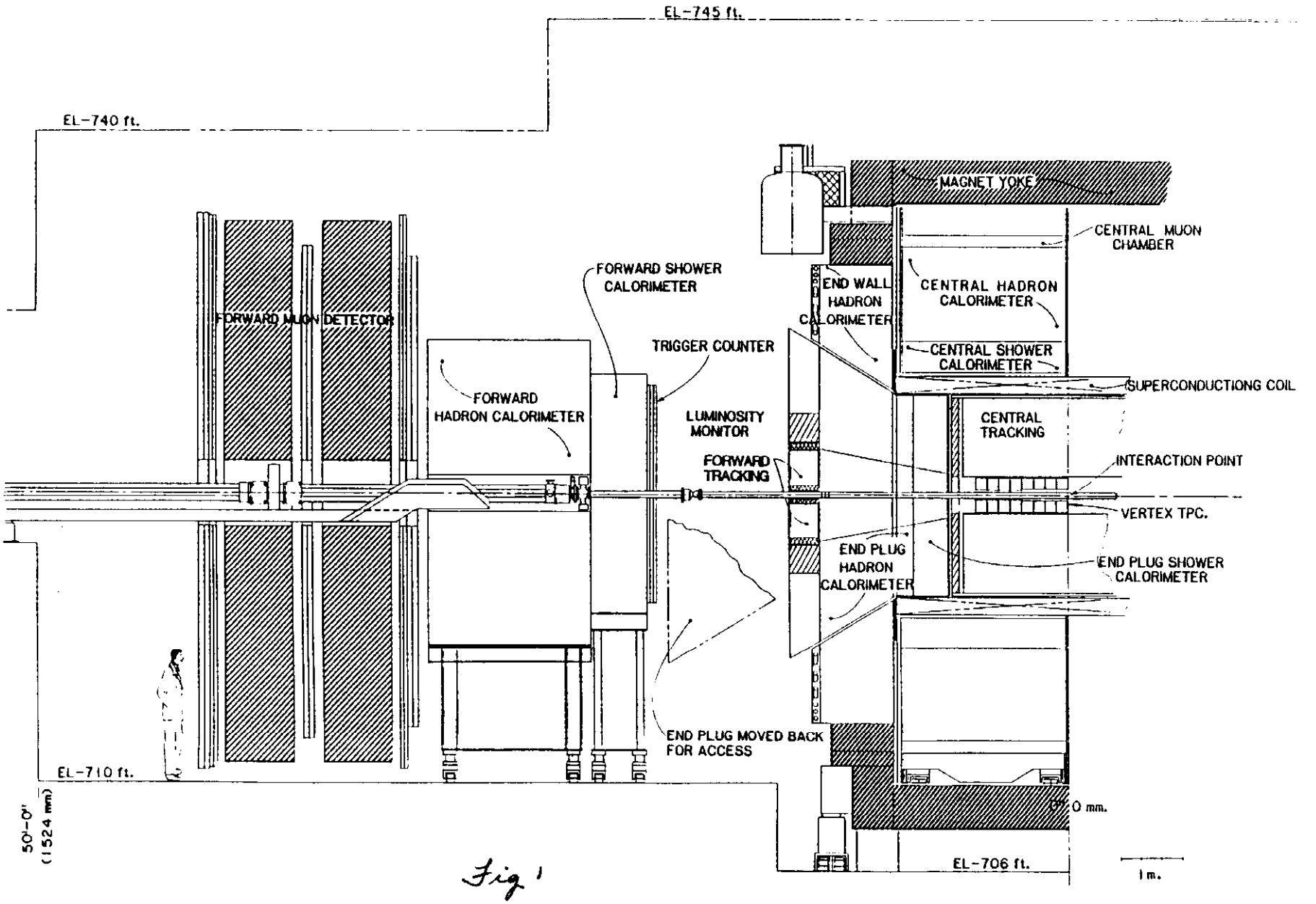
EL-745 ft.
EL-740 ft.
MAGNET YOKE
CENTRAL MUON CHAMBER
FORWARD SHOWER CALORIMETER
END WALL HADRON CALORIMETER
CENTRAL HADRON CALORIMETER
FORWARD MUON DETECTOR
TRIGGER COUNTER
CENTRAL SHOWER CALORIMETER
SUPERCONDUCTIONG COIL
FORWARD HADRON CALORIMETER
LUMINOSITY MONITOR
CENTRAL TRACKING
FORWARD TRACKING
INTERACTION POINT
VERTEX TPC.
END PLUG HADRON CALORIMETER
END PLUG SHOWER CALORIMETER
END PLUG MOVED BACK FOR ACCESS
EL-710 ft.
50'-0" (1524 mm)
0 mm.
EL-706 ft.
1 m.

Fig 1

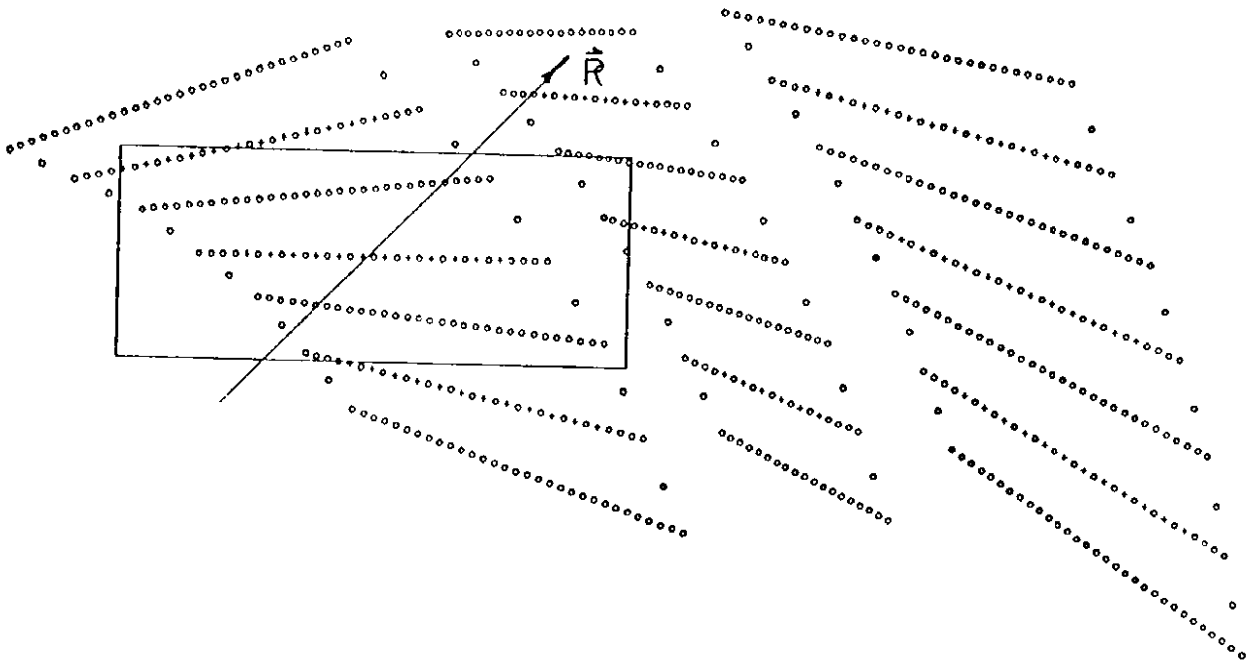

Fig 2a

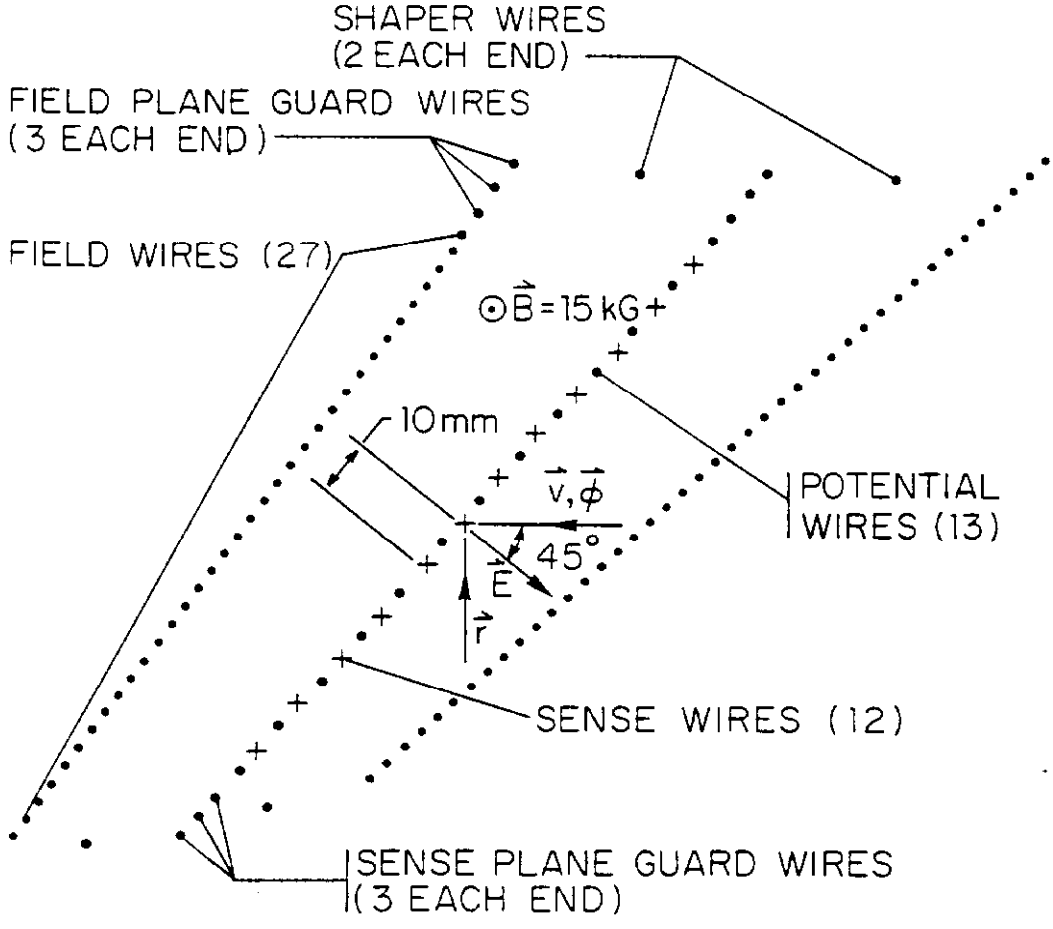
SHAPER WIRES
(2 EACH END)
FIELD PLANE GUARD WIRES
(3 EACH END)
FIELD WIRES (27)
⊙B=15 kG+
10mm
v, φ
45°
E
r
POTENTIAL
WIRES (13)
SENSE WIRES (12)
SENSE PLANE GUARD WIRES
(3 EACH END)

Fig 2 b

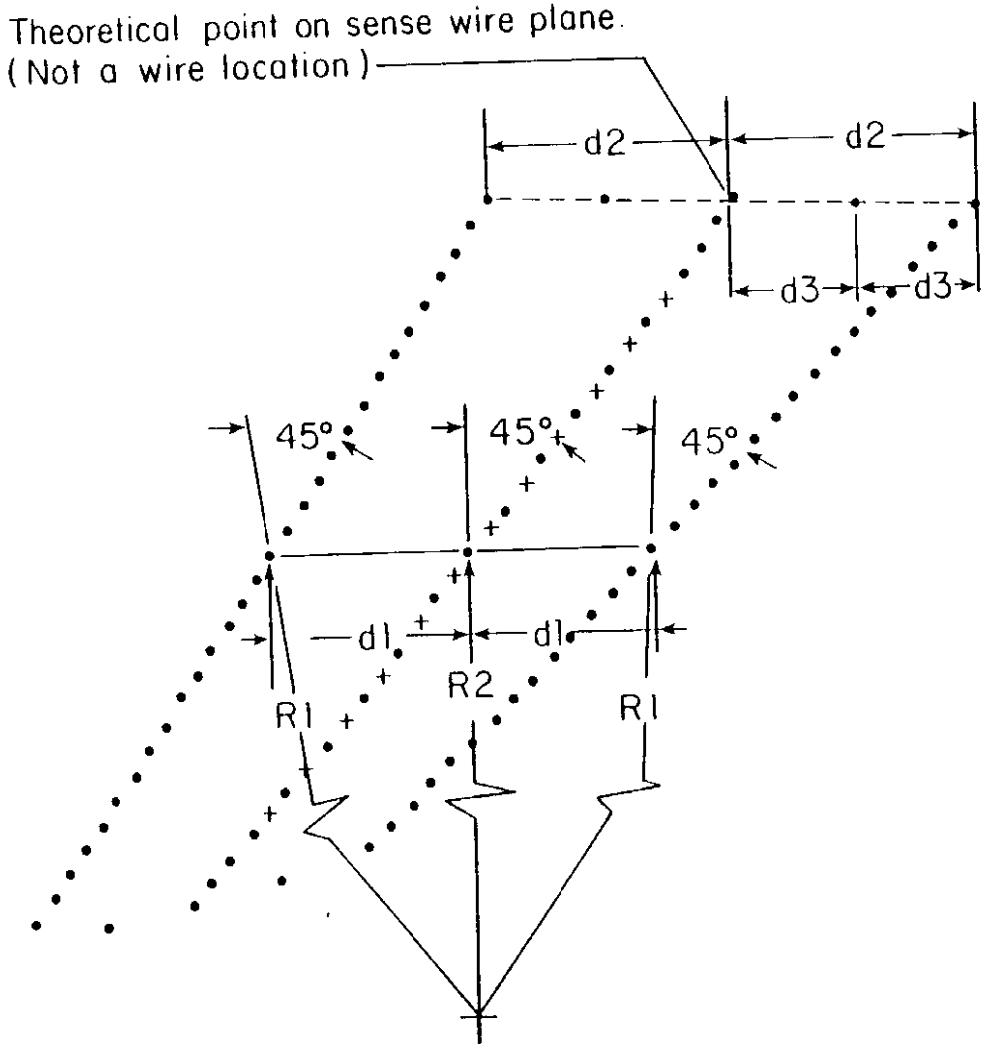
Theoretical point on sense wire plane.
(Not a wire location)
d2
d2
d3
d3
45°
45°
45°
d1
d1
R1
R2
R1

Fig 2c

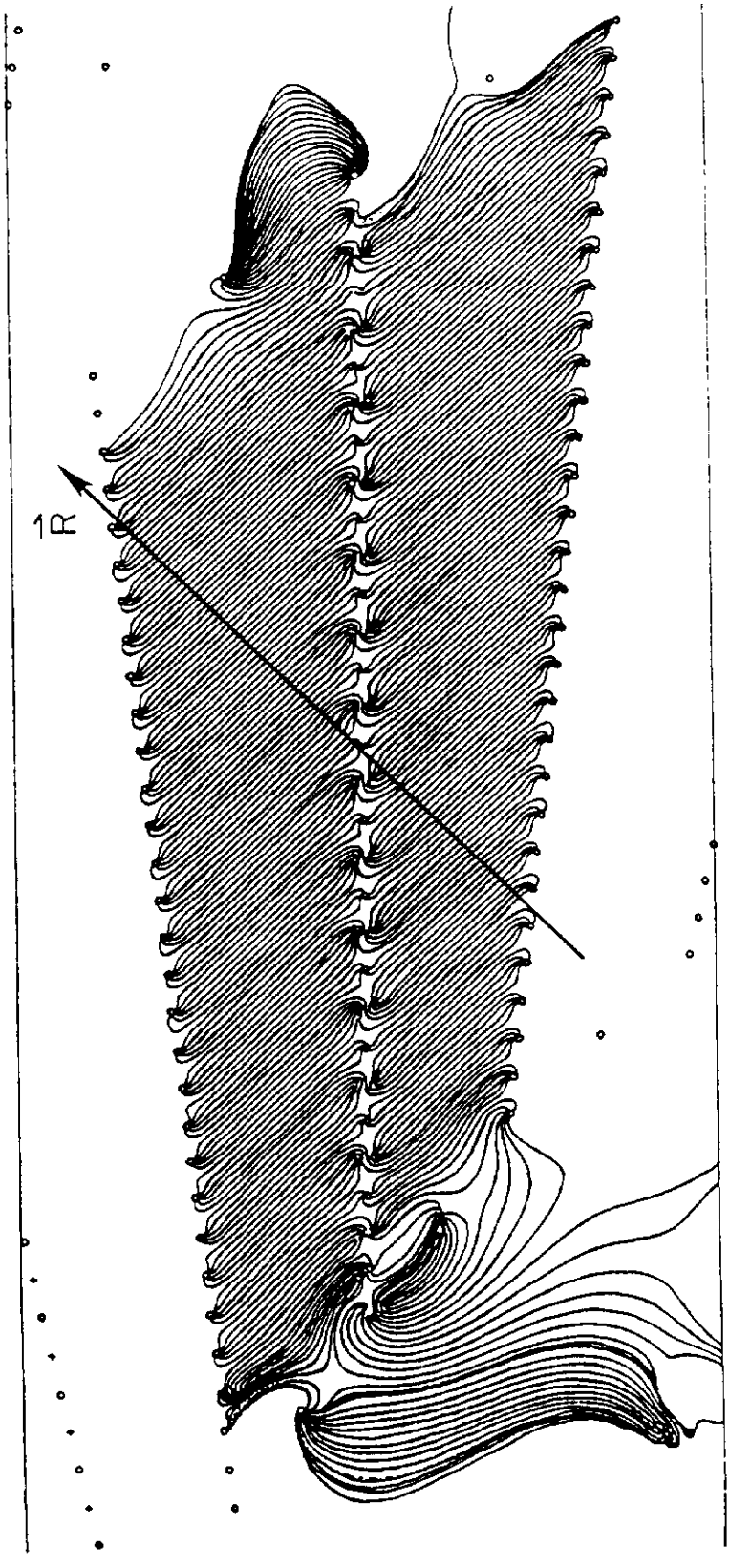

Fig 3

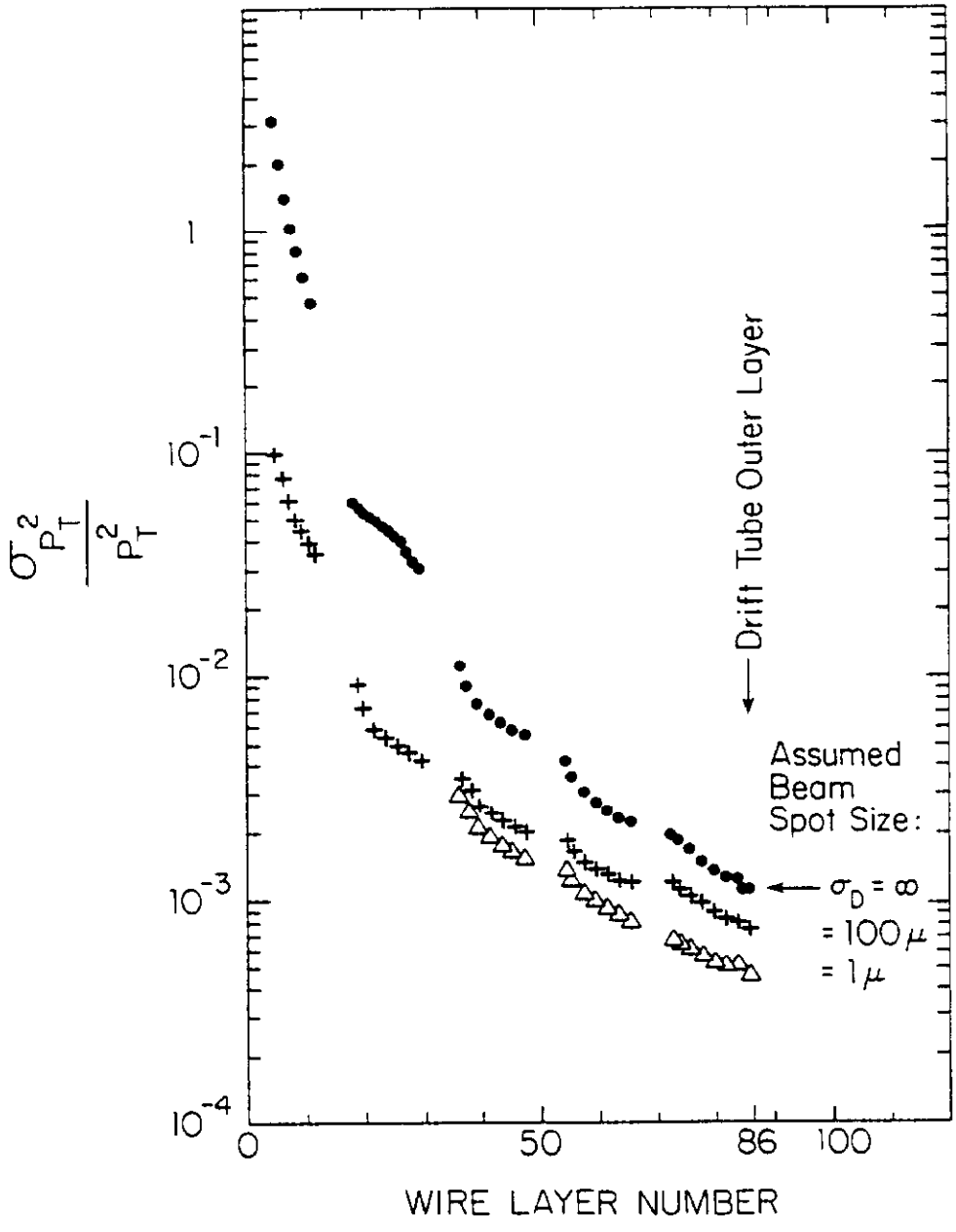
$\frac{\sigma^2_{P_T}}{P_T^2}$
1
10^{-1}
10^{-2}
10^{-3}
10^{-4}
0
50
86
100
WIRE LAYER NUMBER
Drift Tube Outer Layer
Assumed
Beam
Spot Size:
$\sigma_D = \infty$
$= 100\mu$
$= 1\mu$

Fig 4a

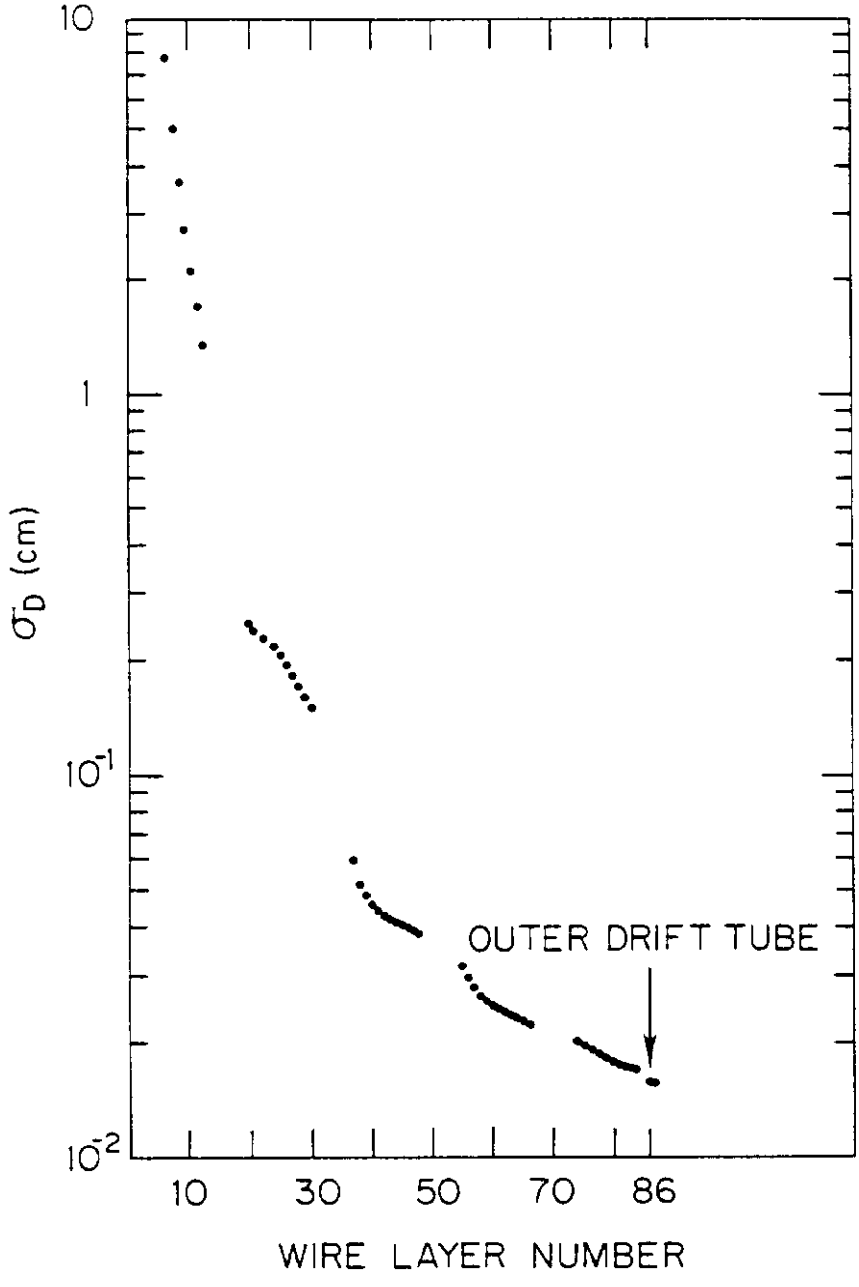
10
1
10^{-1}
10^{-2}
σ_D (cm)
OUTER DRIFT TUBE
10
30
50
70
86
WIRE LAYER NUMBER

Fig 4 a

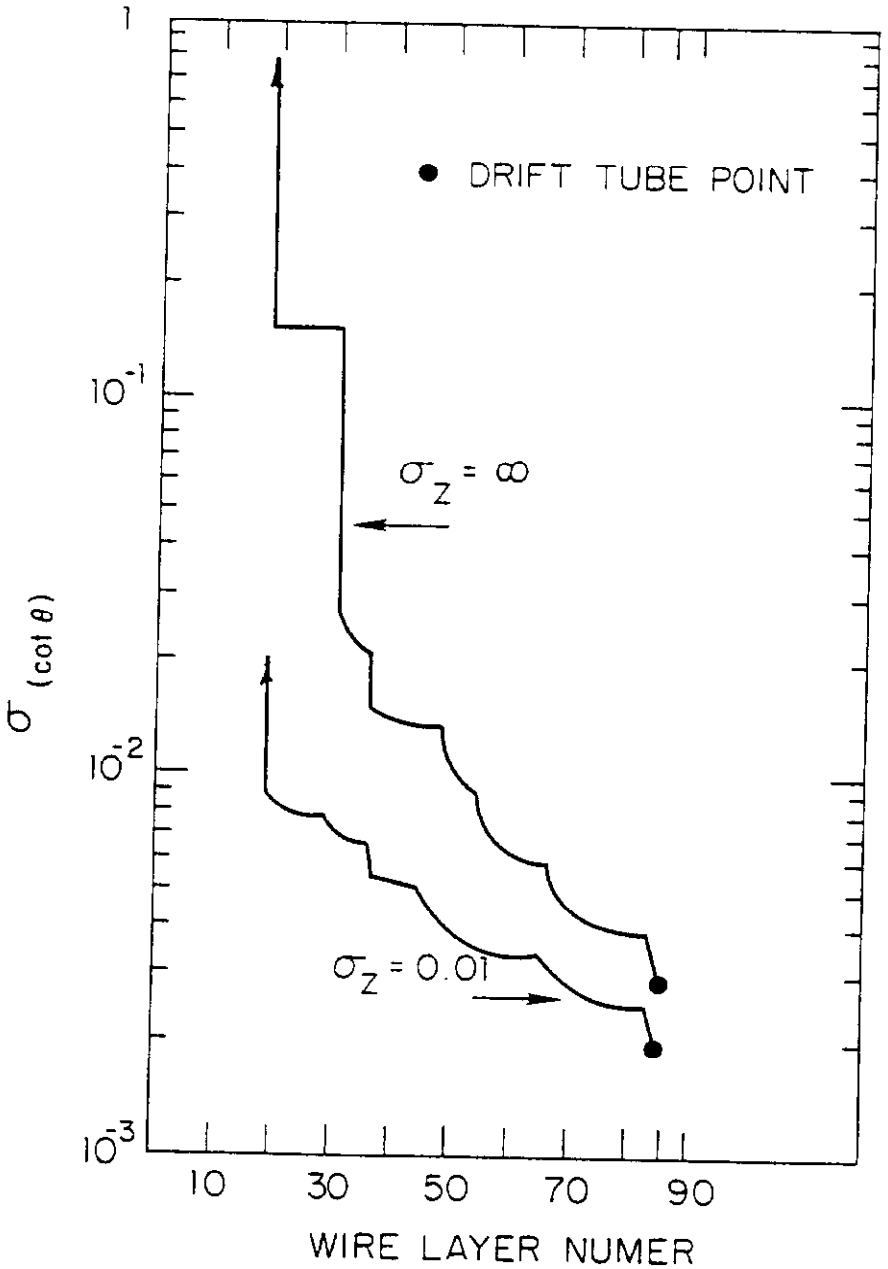
1
10^{-1}
10^{-2}
10^{-3}
$\sigma_{(\cot\theta)}$
DRIFT TUBE POINT
$\sigma_z = \infty$
$\sigma_z = 0.01$
10
30
50
70
90
WIRE LAYER NUMER

Fig 4c

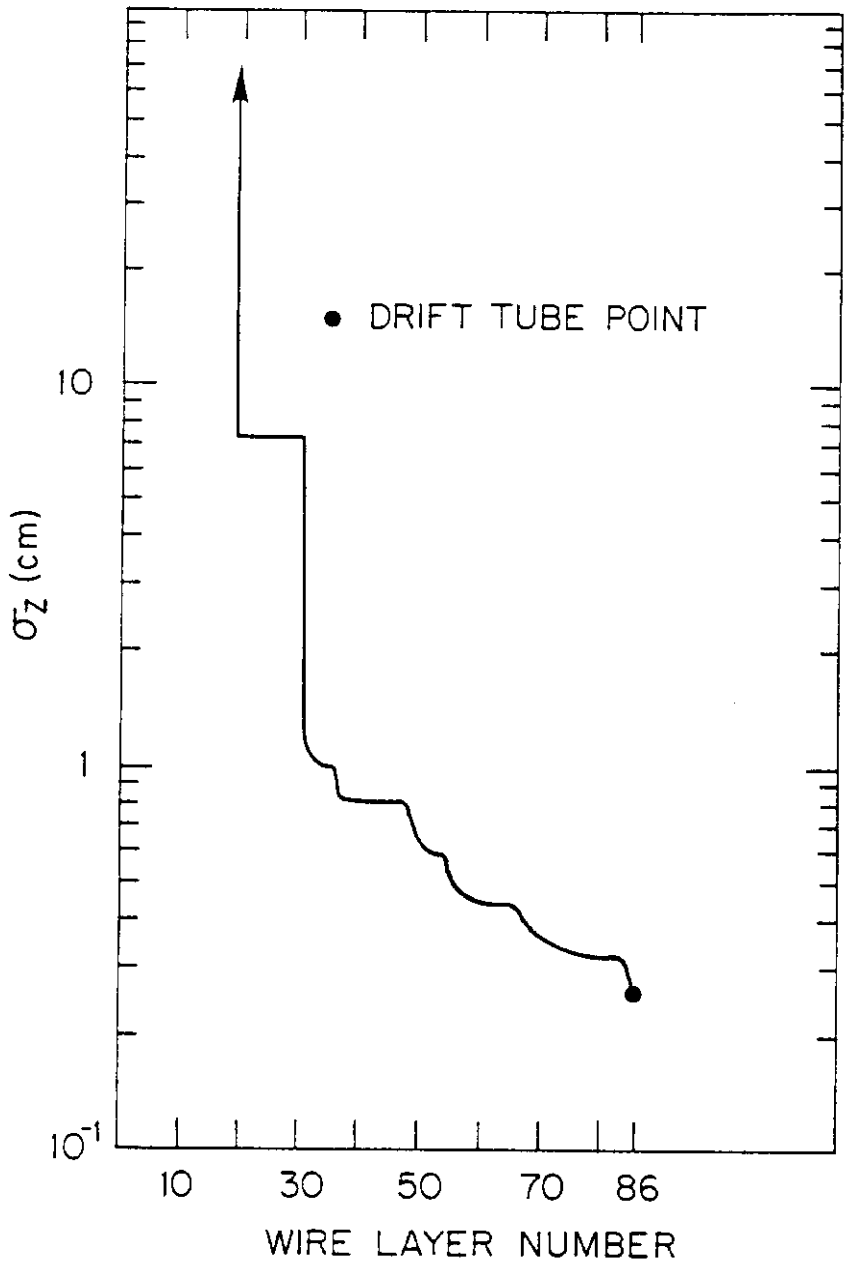
DRIFT TUBE POINT
10
1
10^{-1}
σ_z (cm)
10
30
50
70
86
WIRE LAYER NUMBER

Fig 4d

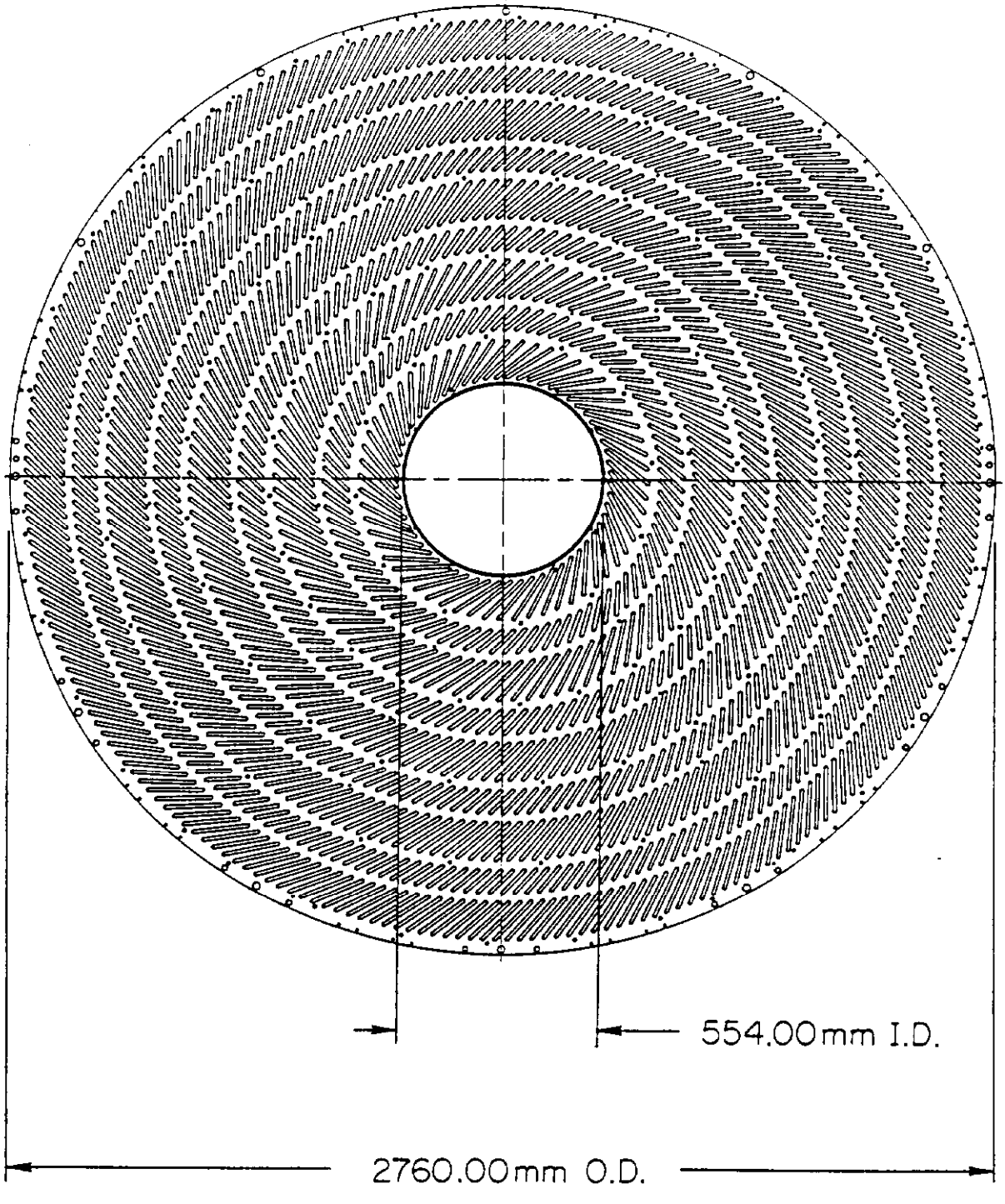

fig 5

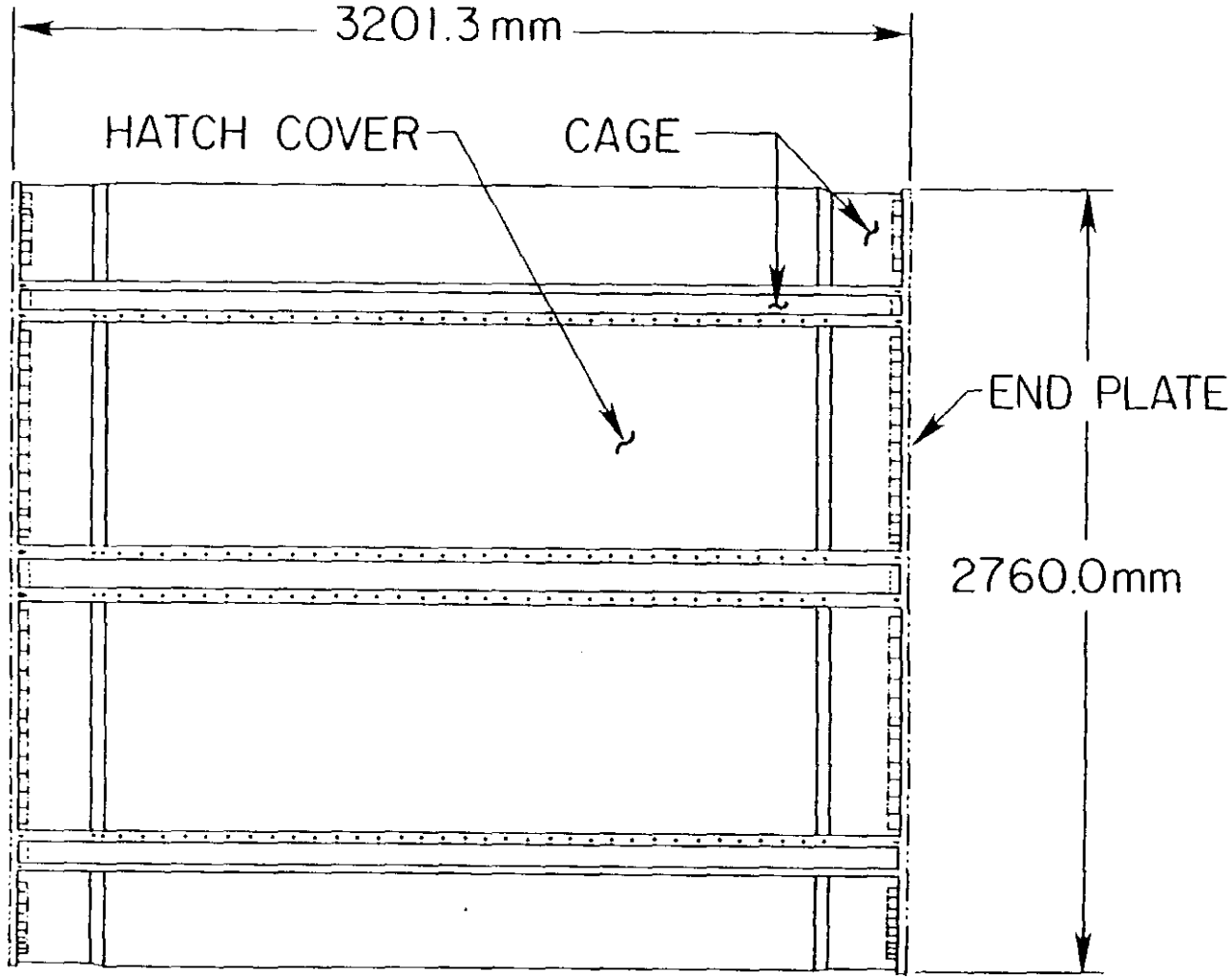

C.T.C. SIDE VIEW

Fig 6

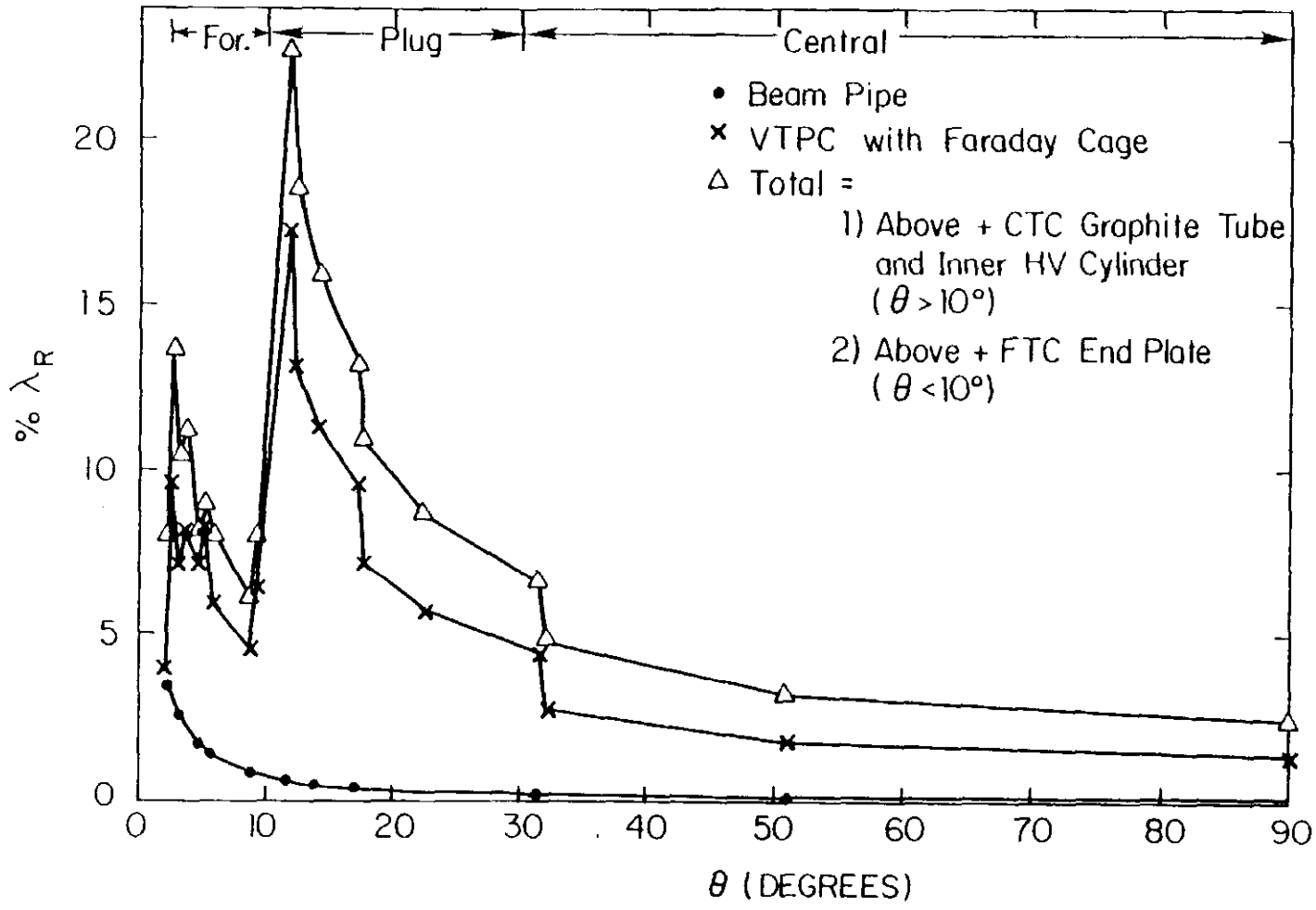
For.
Plug
Central
• Beam Pipe
× VTPC with Faraday Cage
△ Total =
1) Above + CTC Graphite Tube and Inner HV Cylinder (θ > 10°)
2) Above + FTC End Plate (θ < 10°)
% λR
0
5
10
15
20
0
10
20
30
40
50
60
70
80
90
θ (DEGREES)

Fig 7

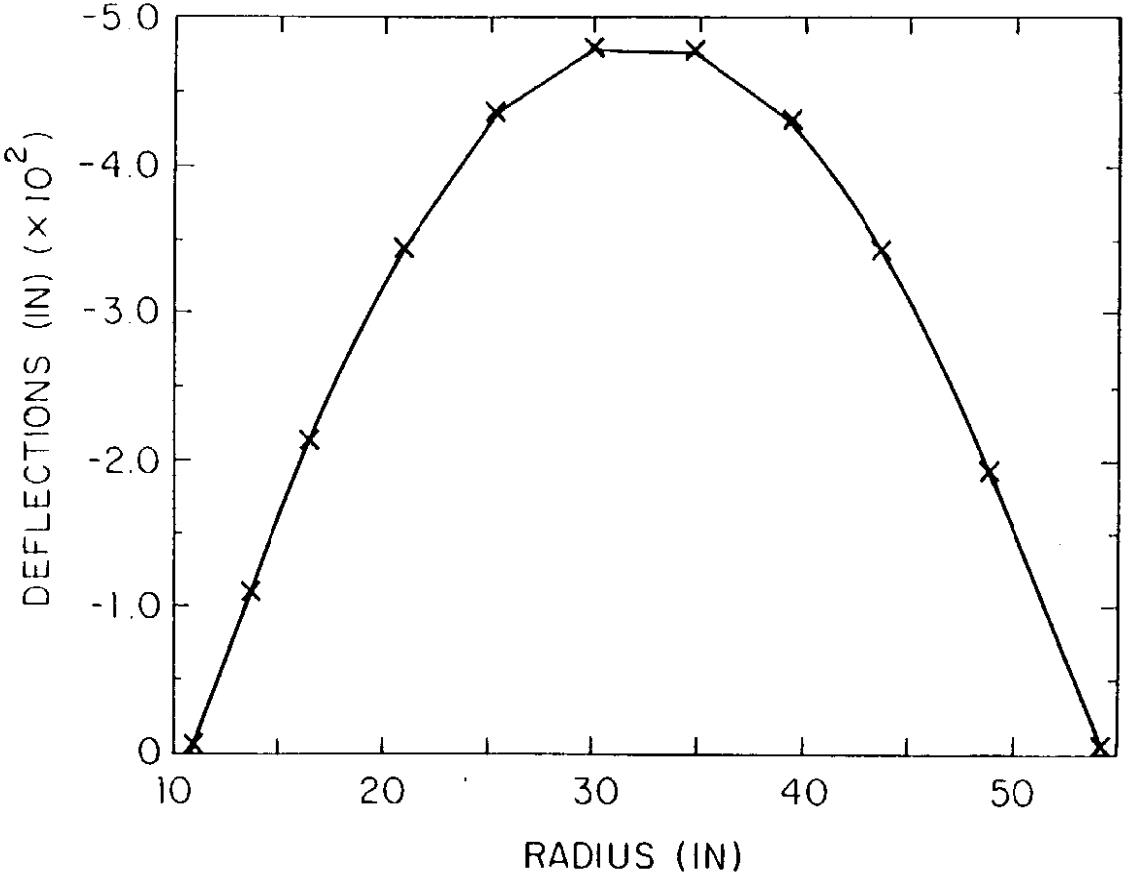

Fig 8

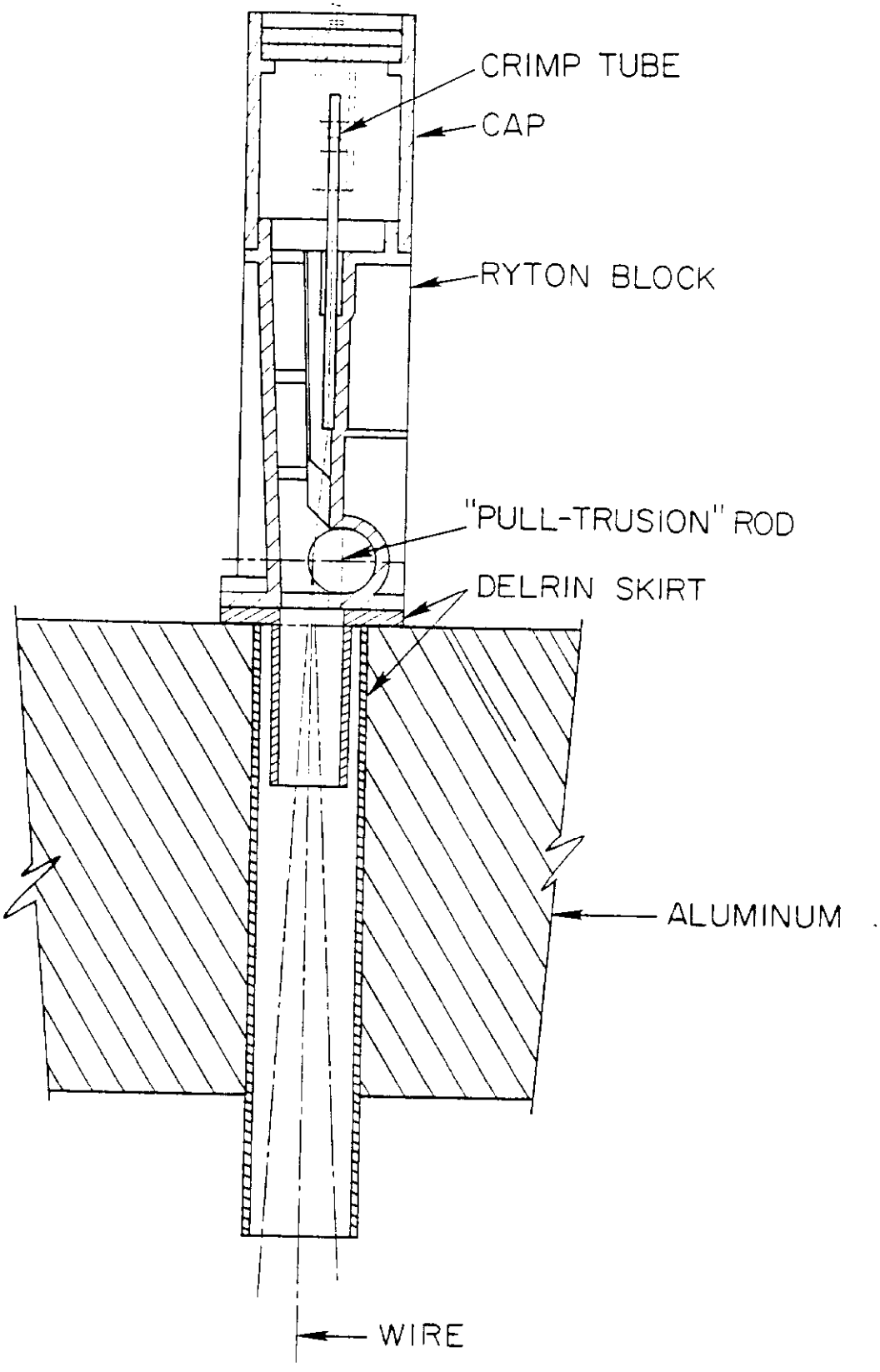
CRIMP TUBE
CAP
RYTON BLOCK
"PULL-TRUSION" ROD
DELRIN SKIRT
ALUMINUM
WIRE

Fig 9a

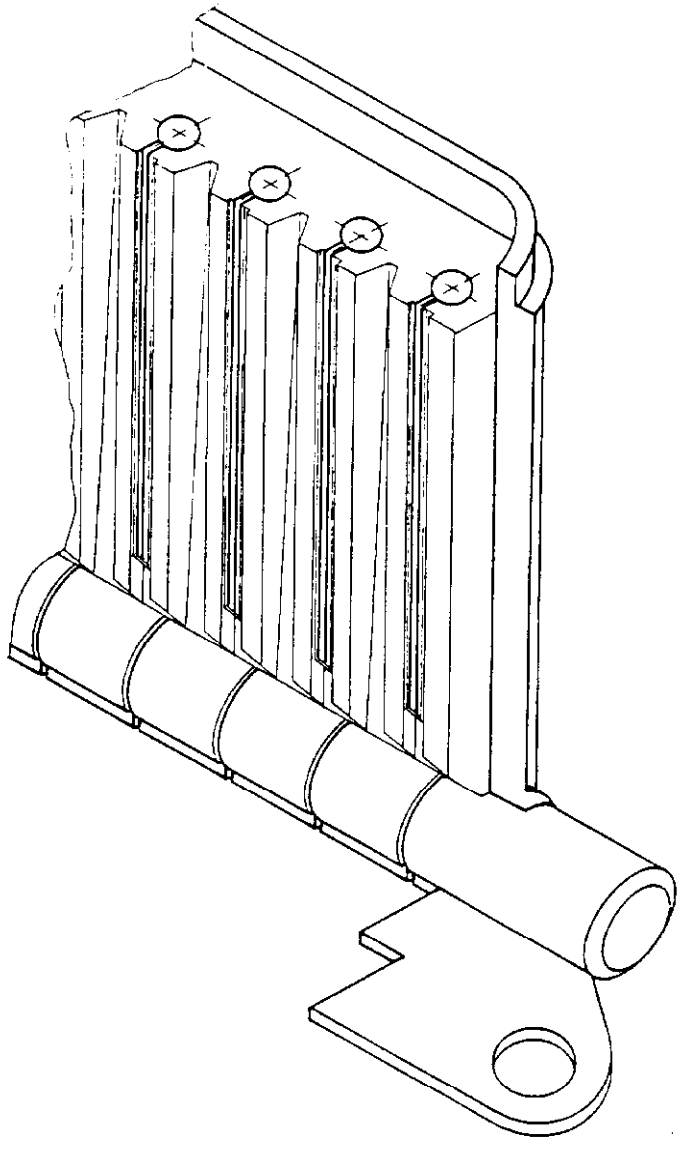

Fig 9 b

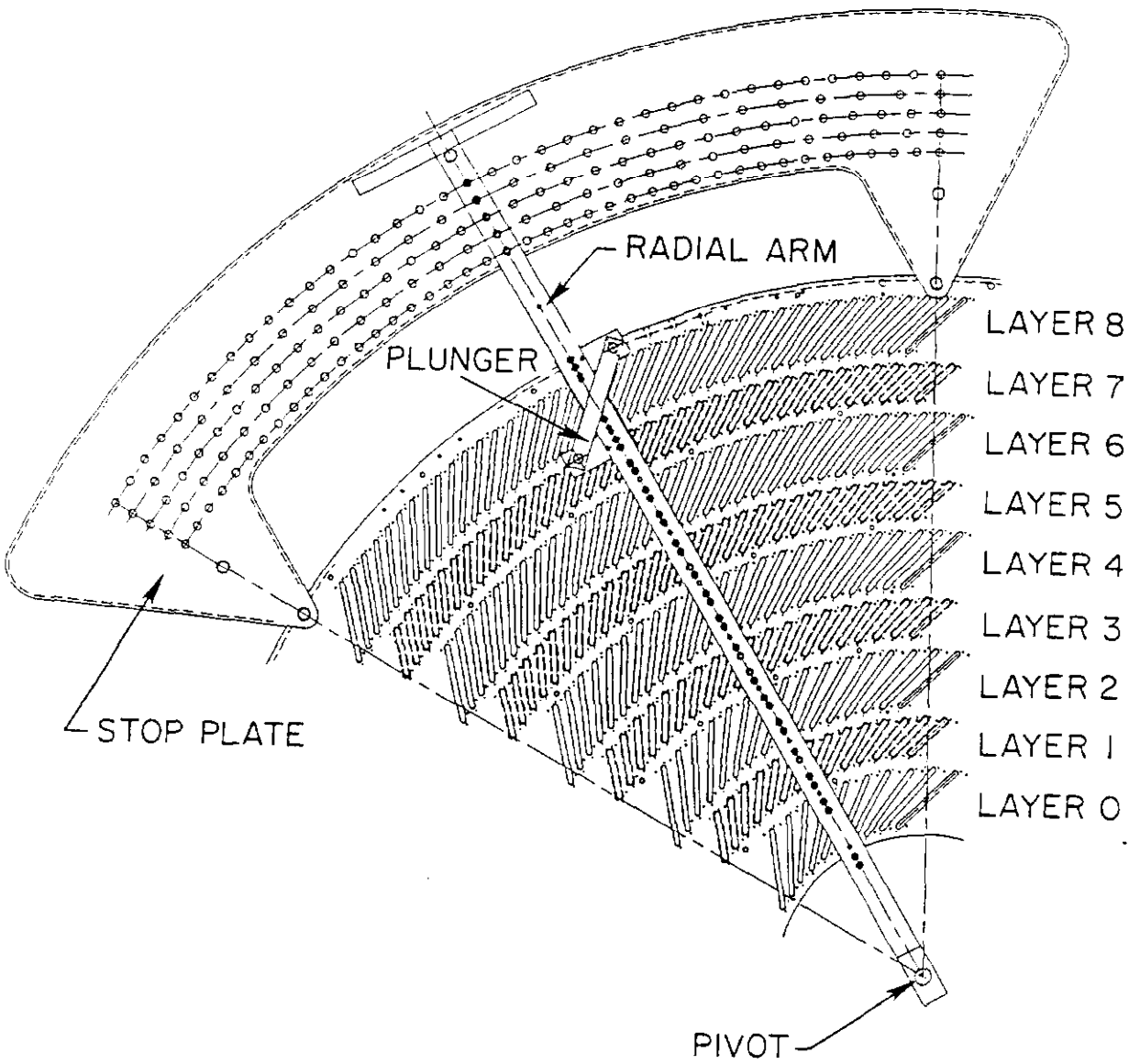
RADIAL ARM
PLUNGER
LAYER 8
LAYER 7
LAYER 6
LAYER 5
LAYER 4
LAYER 3
LAYER 2
LAYER 1
LAYER 0
STOP PLATE
PIVOT

Fig 10a

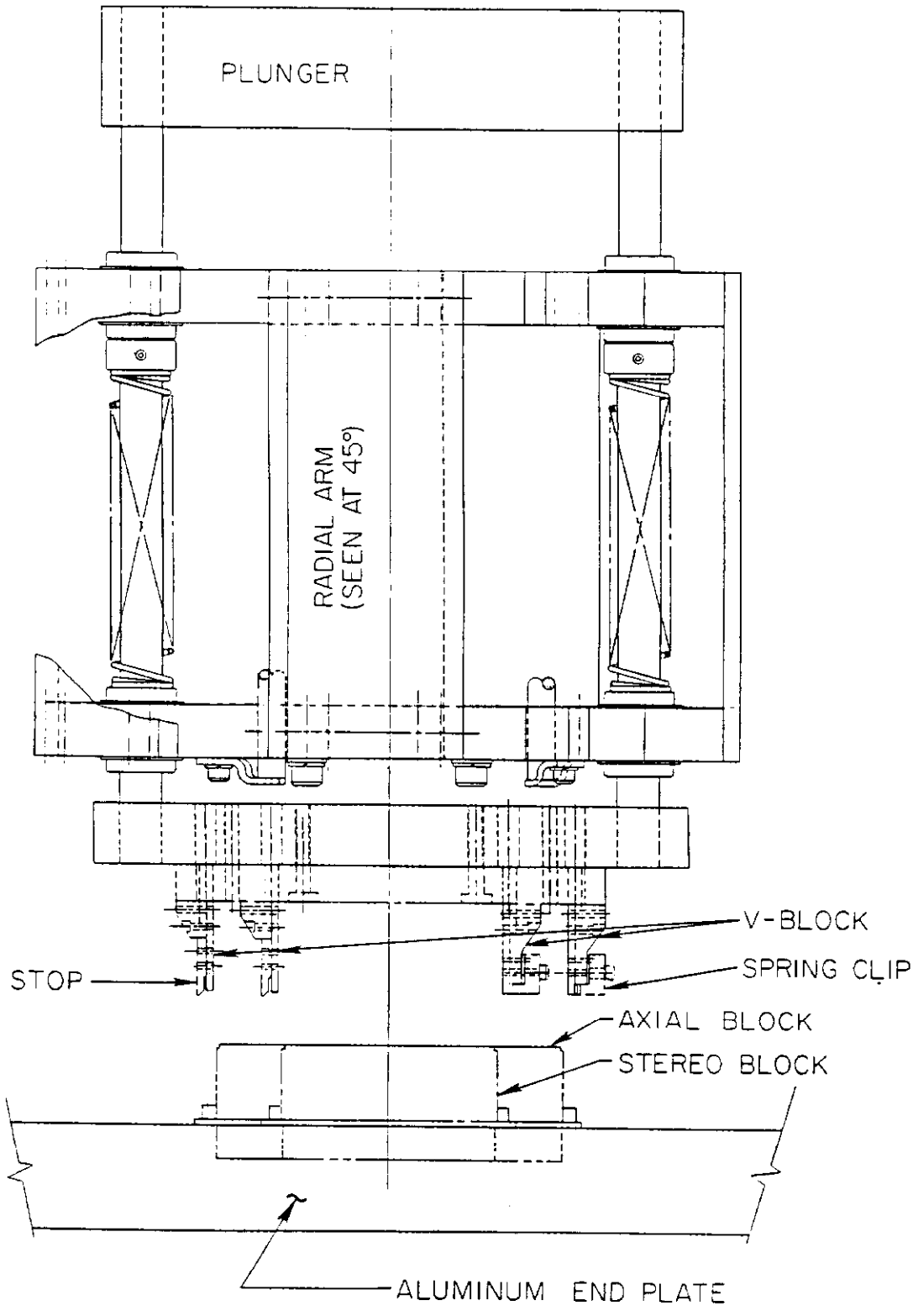
PLUNGER
RADIAL ARM
(SEEN AT 45°)
V-BLOCK
STOP
SPRING CLIP
AXIAL BLOCK
STEREO BLOCK
ALUMINUM END PLATE

Fig 10 b

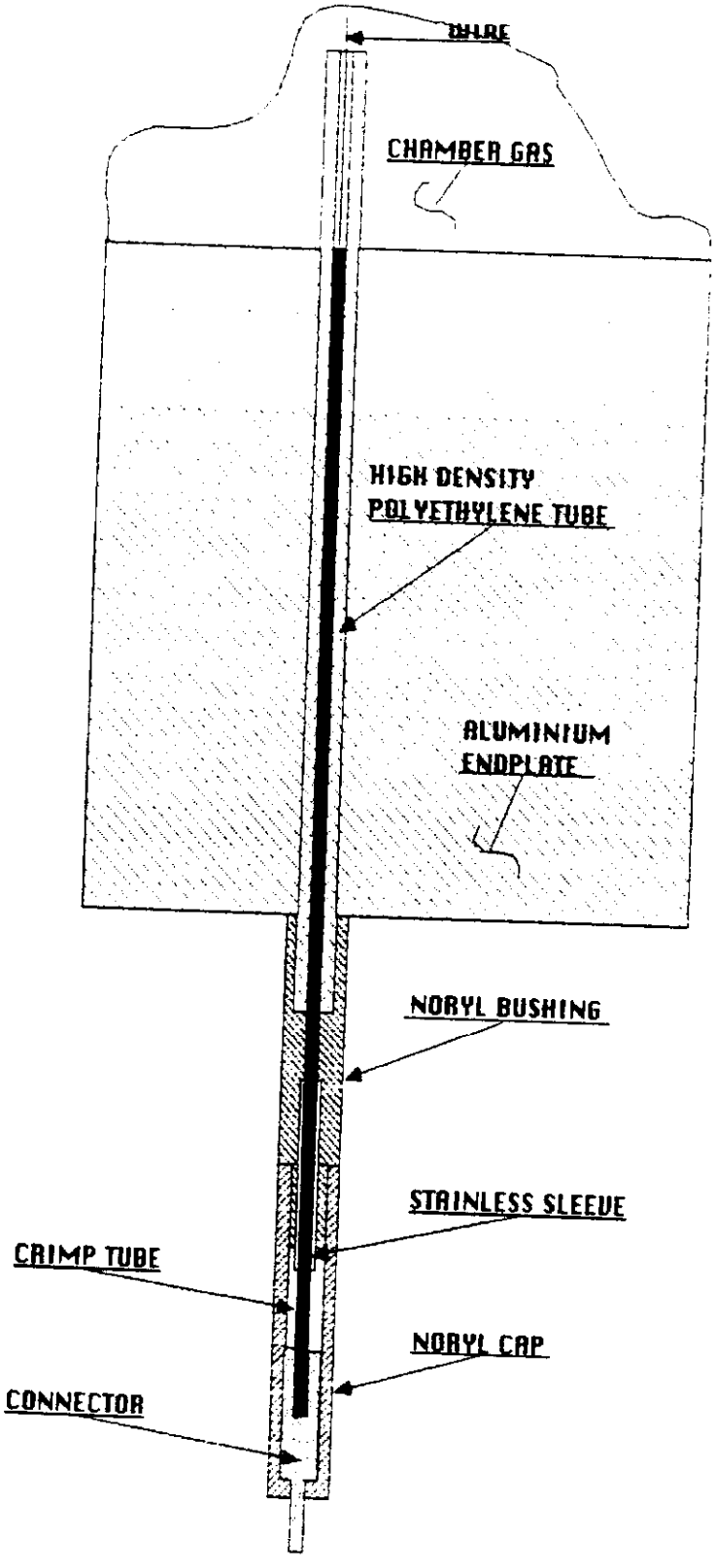
CHAMBER GAS
HIGH DENSITY
POLYETHYLENE TUBE
ALUMINIUM
ENDPLATE
NORYL BUSHING
STAINLESS SLEEVE
CRIMP TUBE
NORYL CAP
CONNECTOR

Fig 11

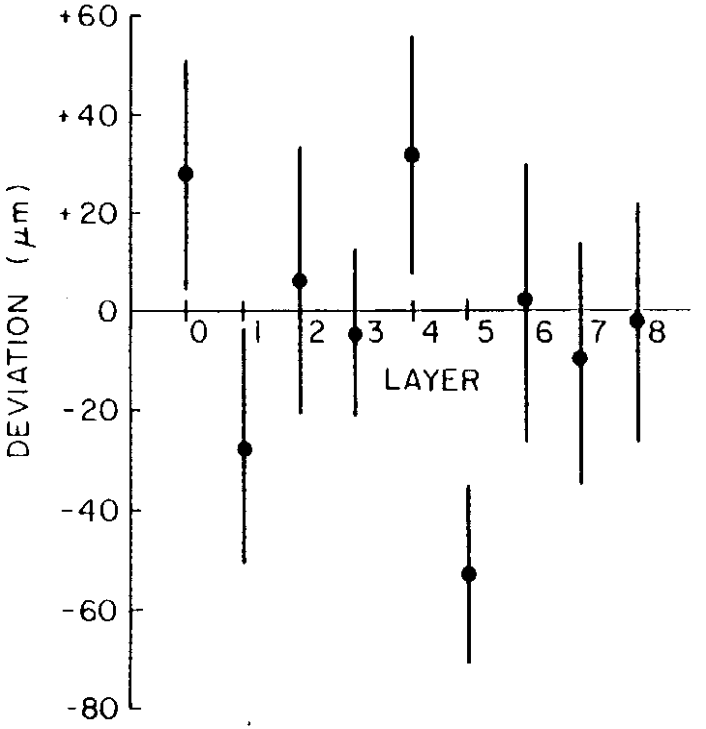

Fig 12

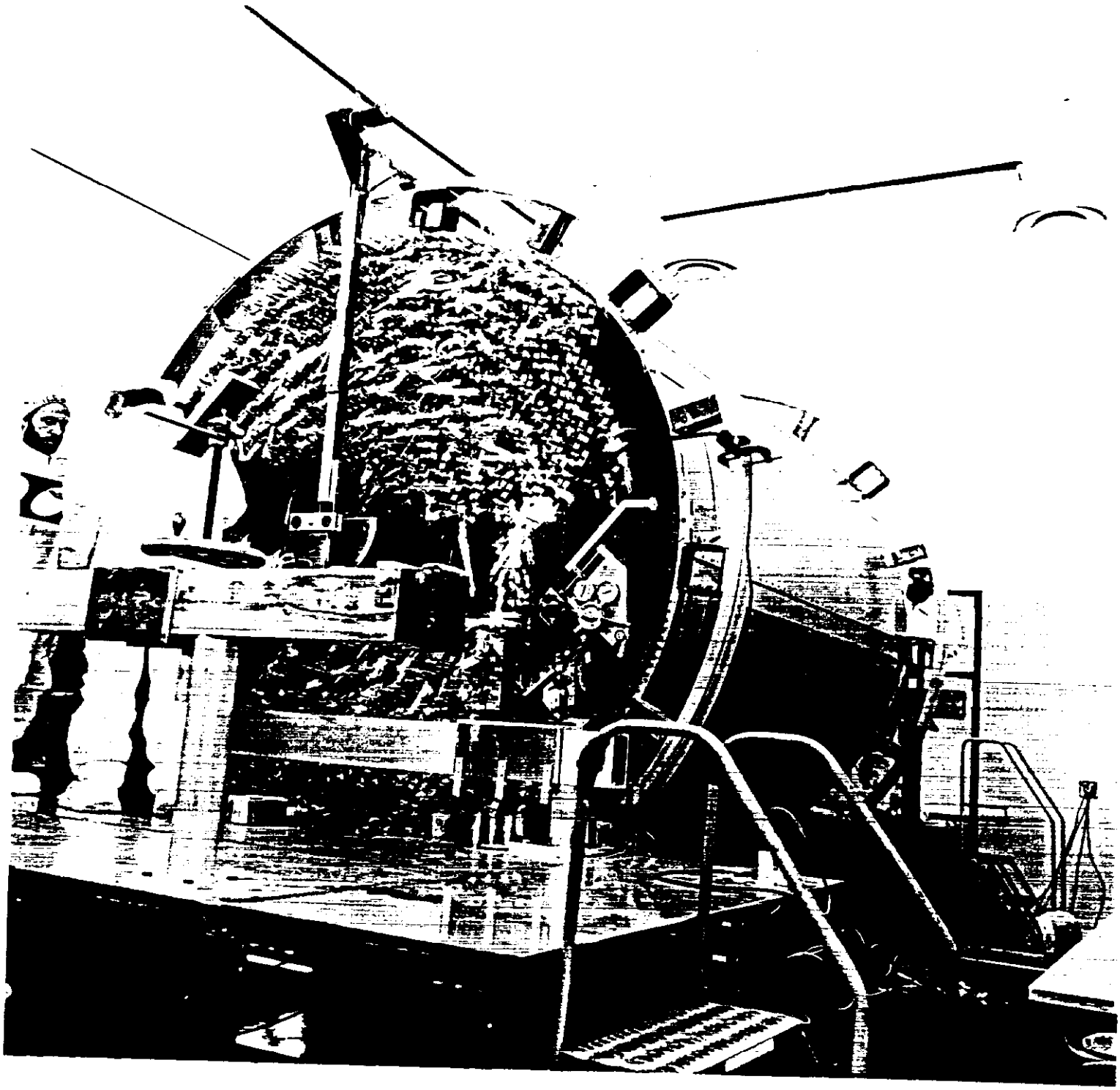

Fig 13

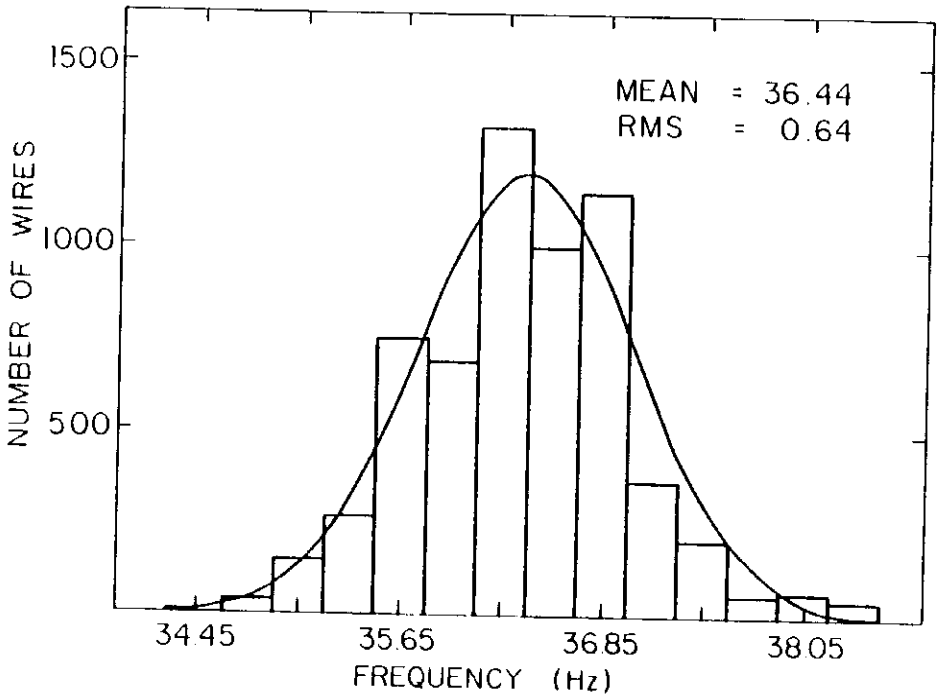
1500
1000
500
NUMBER OF WIRES
MEAN = 36.44
RMS = 0.64
34.45
35.65
36.85
38.05
FREQUENCY (Hz)

Fig 14

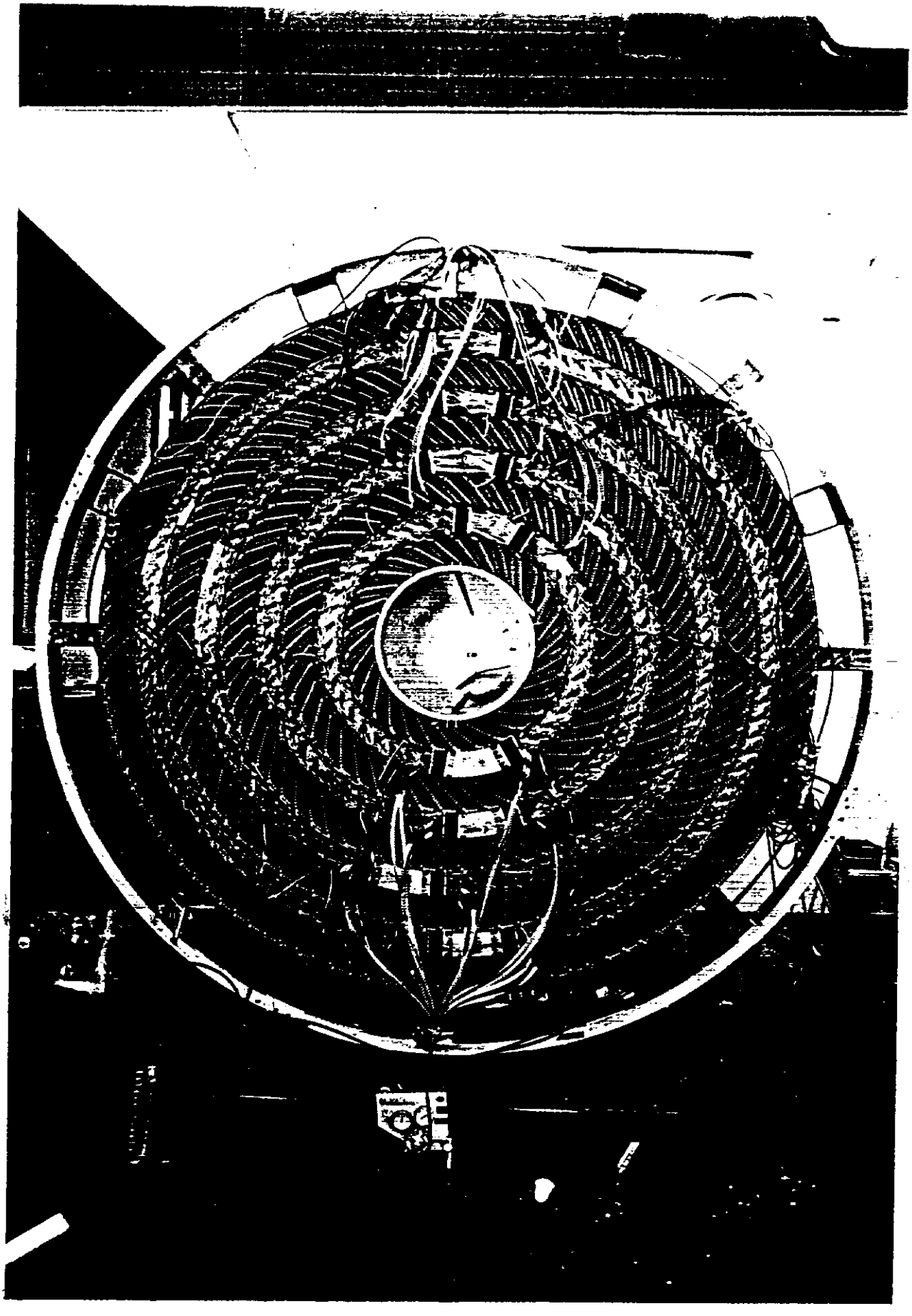

Fig 15a

Fig 15-b

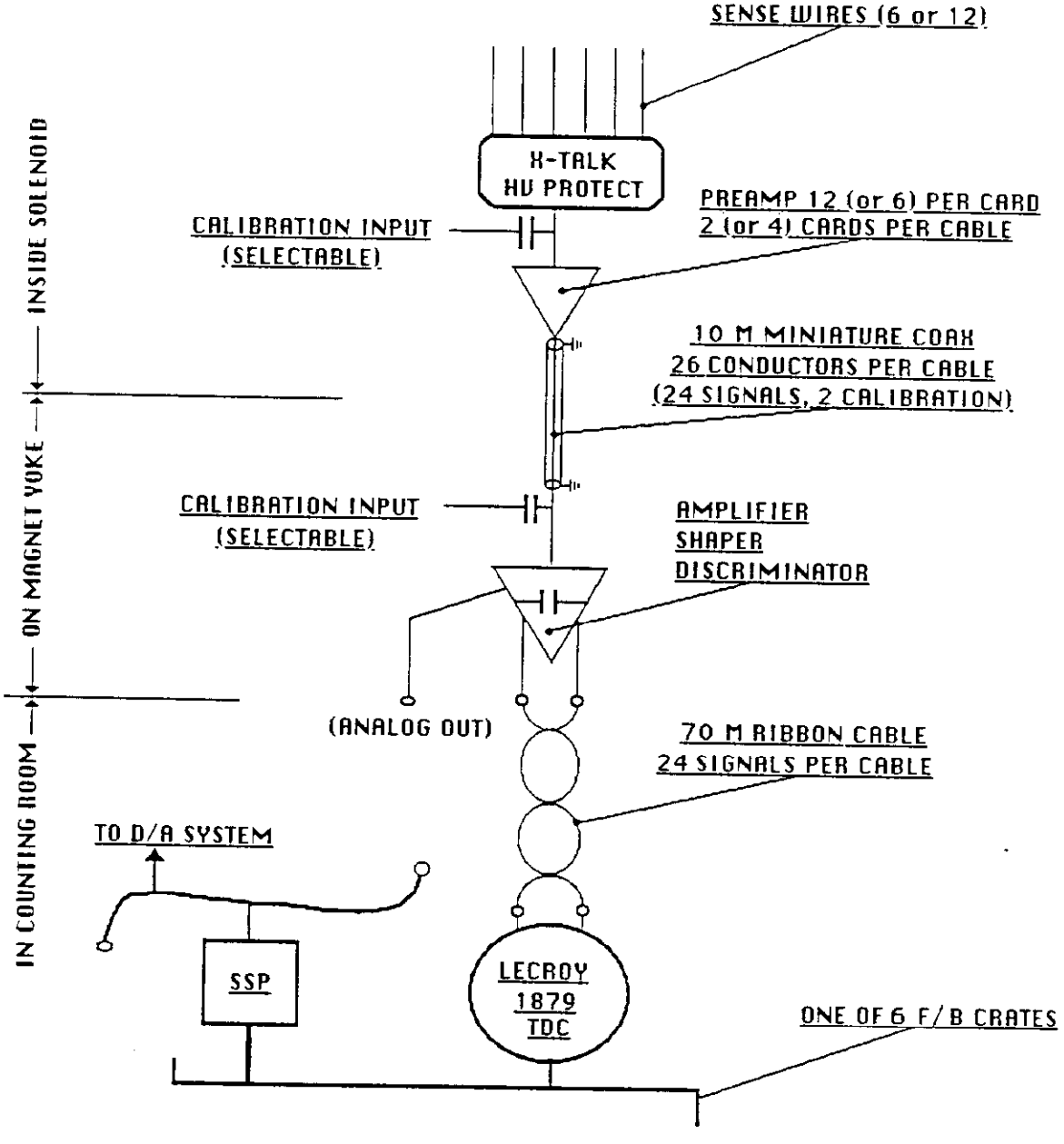
SENSE WIRES (6 or 12)
X-TALK
HV PROTECT
PREAMP 12 (or 6) PER CARD
2 (or 4) CARDS PER CABLE
CALIBRATION INPUT
(SELECTABLE)
10 M MINIATURE COAX
26 CONDUCTORS PER CABLE
(24 SIGNALS, 2 CALIBRATION)
CALIBRATION INPUT
(SELECTABLE)
AMPLIFIER
SHAPER
DISCRIMINATOR
(ANALOG OUT)
70 M RIBBON CABLE
24 SIGNALS PER CABLE
TO D/A SYSTEM
SSP
LECROY
1879
TDC
ONE OF 6 F/B CRATES
IN COUNTING ROOM
ON MAGNET YOKE
INSIDE SOLENOID

Fig 16

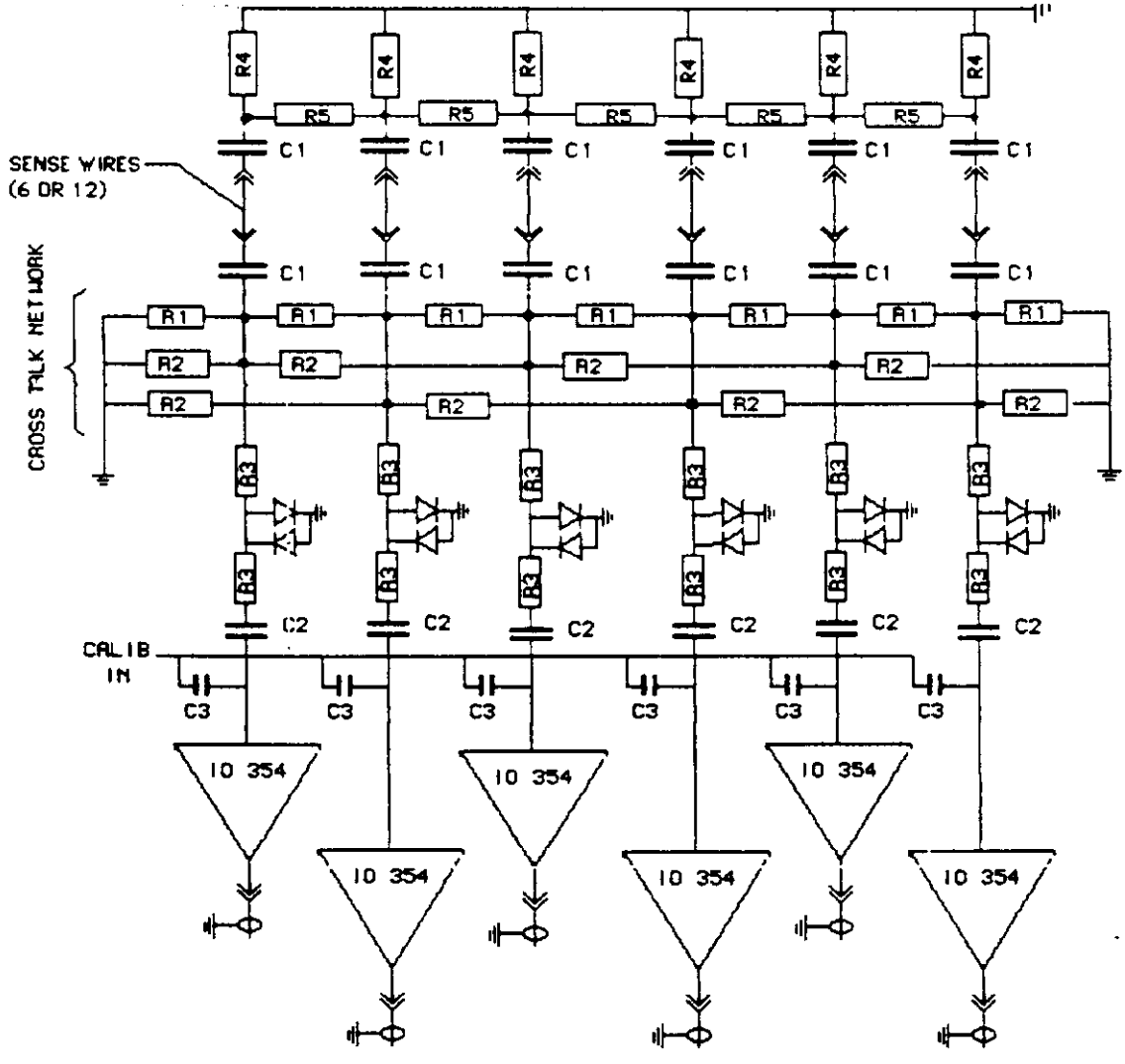

ALL RESISTORS 1/8 W	
ALL DIODES 1N914	
R1	2700
R2	6800
R3	50
R4	590
R5	10K
C1	1200pF, 3KV
C2	0.1μF, 100V
C3	0.3 pF

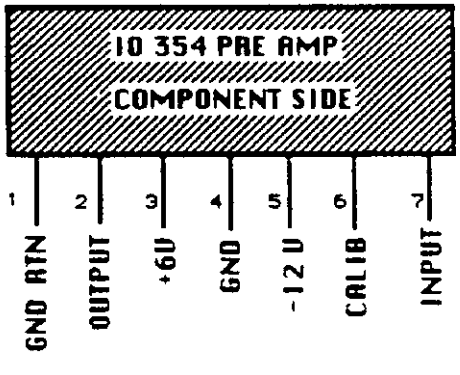

Fig 17

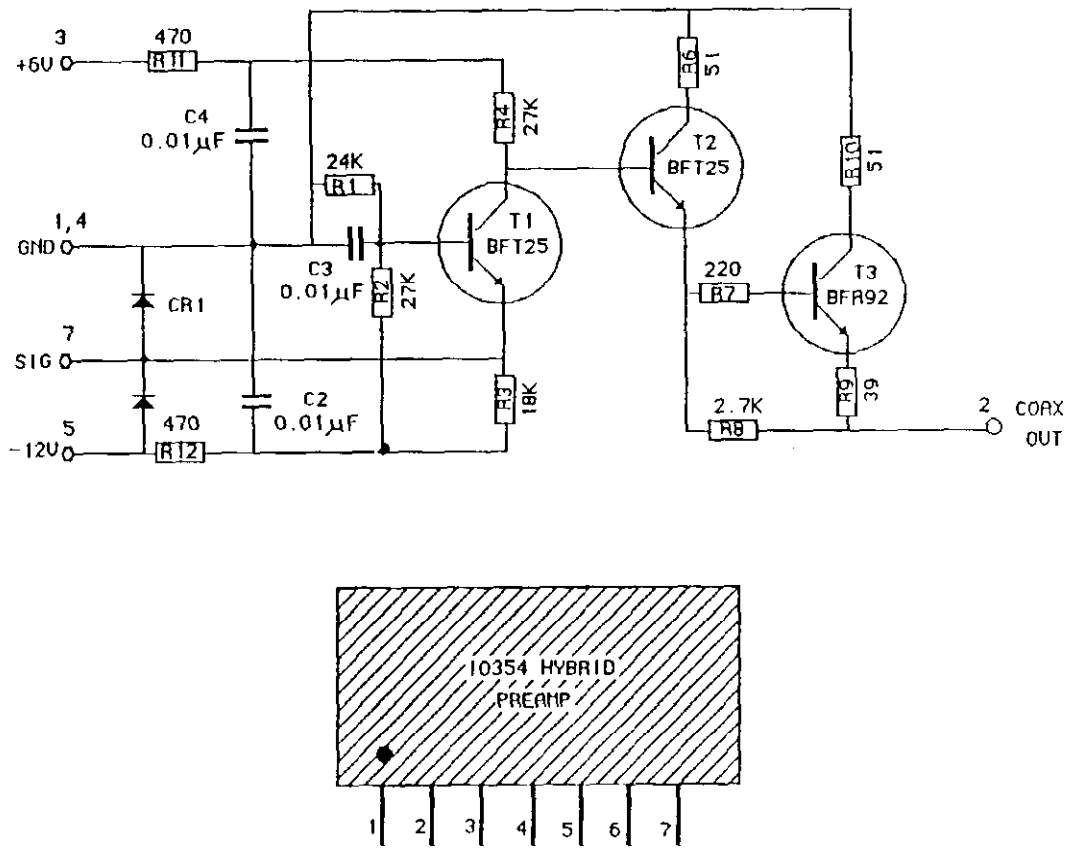
3
+6V
470
R11
C4
0.01µF
24K
R1
R4
27K
T1
BFT25
T2
BFT25
R6
51
R10
51
1,4
GND
C3
0.01µF
R2
27K
220
R7
T3
BFR92
CR1
7
SIG
R3
18K
R9
39
2.7K
R8
2
COAX
OUT
5
-12V
470
R12
C2
0.01µF
10354 HYBRID
PREAMP
1
2
3
4
5
6
7

Fig 18

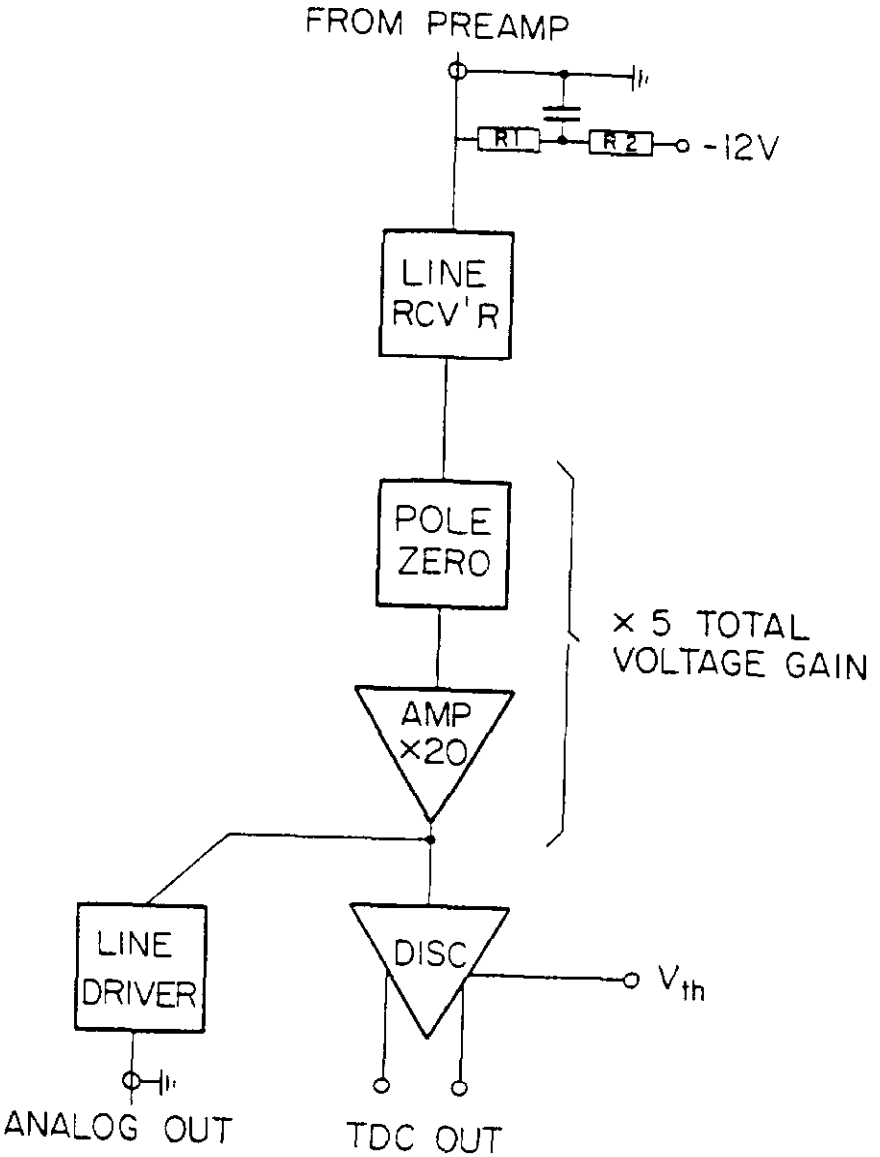
FROM PREAMP
R1
R2
-12V
LINE RCV'R
POLE ZERO
× 5 TOTAL VOLTAGE GAIN
AMP ×20
LINE DRIVER
DISC
V_{th}
ANALOG OUT
TDC OUT

Fig 19

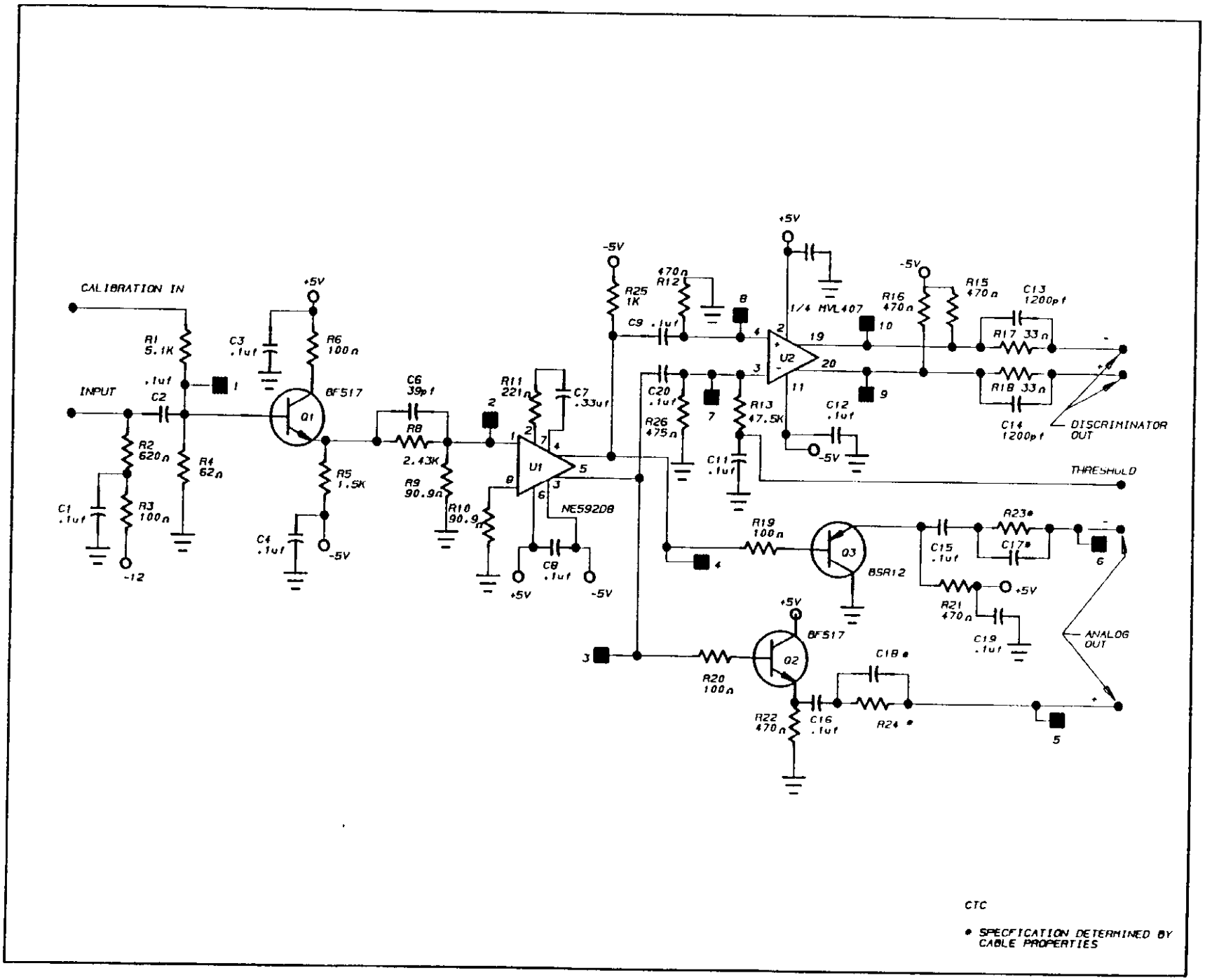
CALIBRATION IN
INPUT
R1 5.1K
.1uf
C2
R2 620n
R4 62n
C1 .1uf
R3 100n
-12
C3 .1uf
+5V
R6 100n
BF517
Q1
R5 1.5K
C4 .1uf
-5V
C6 39pf
R8 2.43K
R9 90.9n
R10 90.9n
R11 221n
C7 .33uf
U1
NE592D8
C8 .1uf
+5V
-5V
R25 1K
-5V
470n R12
C9 .1uf
+5V
1/4 HVL407
U2
C20 .1uf
R26 475n
R13 47.5K
C11 .1uf
C12 .1uf
-5V
R16 470n
-5V
R15 470n
C13 1200pf
R17 33n
R18 33n
C14 1200pf
DISCRIMINATOR OUT
THRESHOLD
R19 100n
Q3
BSR12
C15 .1uf
R23* C17*
+5V
R21 470n
C19 .1uf
ANALOG OUT
+5V
BF517
Q2
R20 100n
C18*
R22 470n
C16 .1uf
R24*
CTC
* SPECIFICATION DETERMINED BY CABLE PROPERTIES

Fig 20

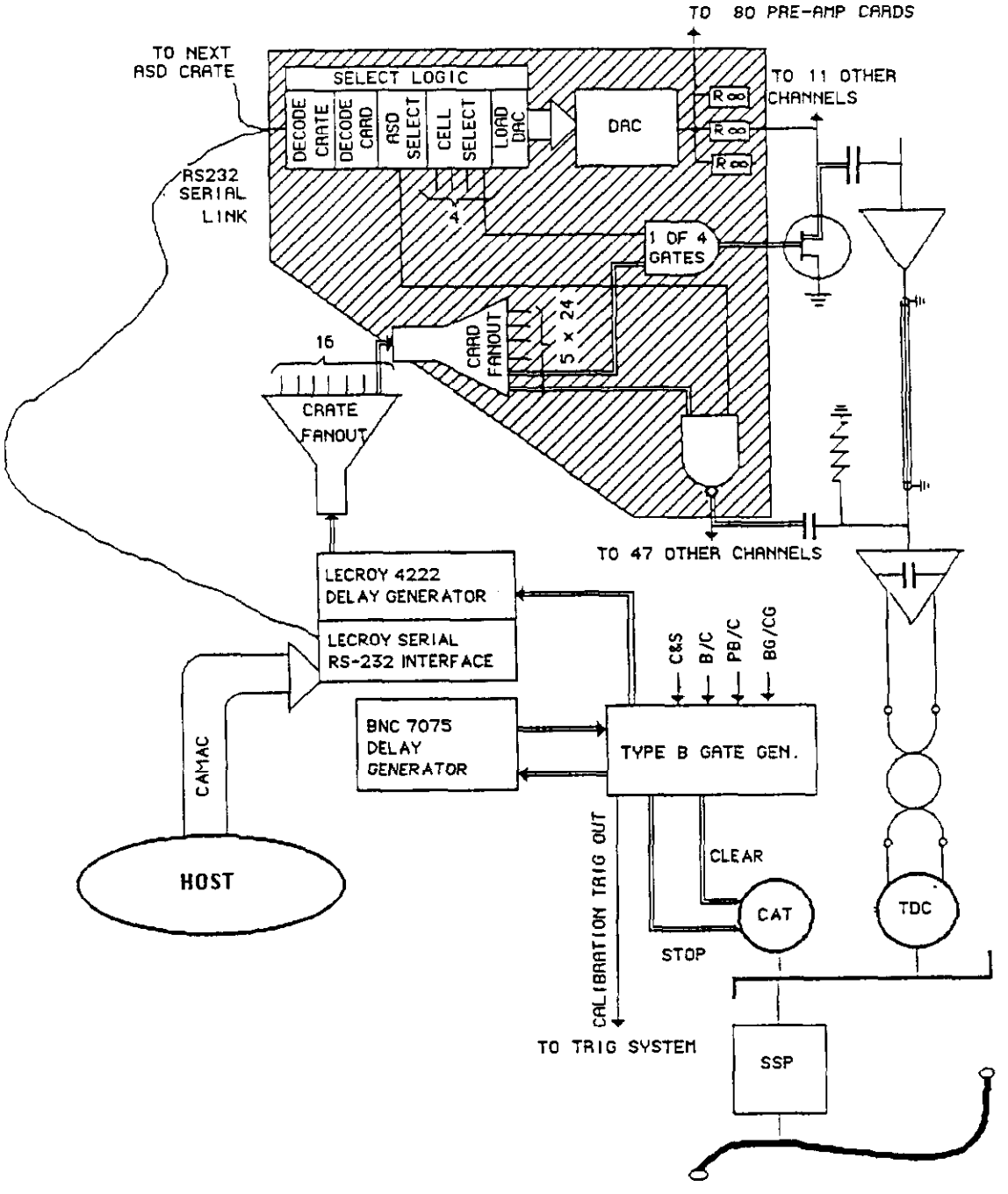
TO 80 PRE-AMP CARDS
TO NEXT ASD CRATE
SELECT LOGIC
DECODE CRATE
DECODE CARD
ASD SELECT
CELL SELECT
LOAD DAC
DAC
TO 11 OTHER CHANNELS
RS232 SERIAL LINK
4
1 OF 4 GATES
CARD FANOUT
5 x 24
16
CRATE FANOUT
TO 47 OTHER CHANNELS
LECROY 4222 DELAY GENERATOR
LECROY SERIAL RS-232 INTERFACE
C&S
B/C
PB/C
BG/CG
BNC 7075 DELAY GENERATOR
TYPE B GATE GEN.
CAMAC
HOST
CLEAR
CAT
TDC
STOP
CALIBRATION TRIG OUT
TO TRIG SYSTEM
SSP

Fig 21

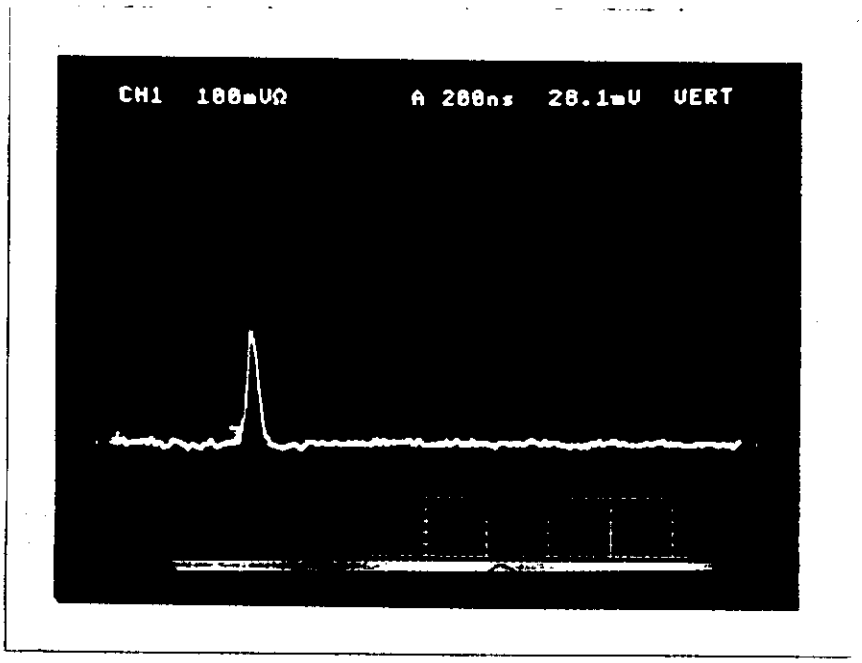

Fig 22a

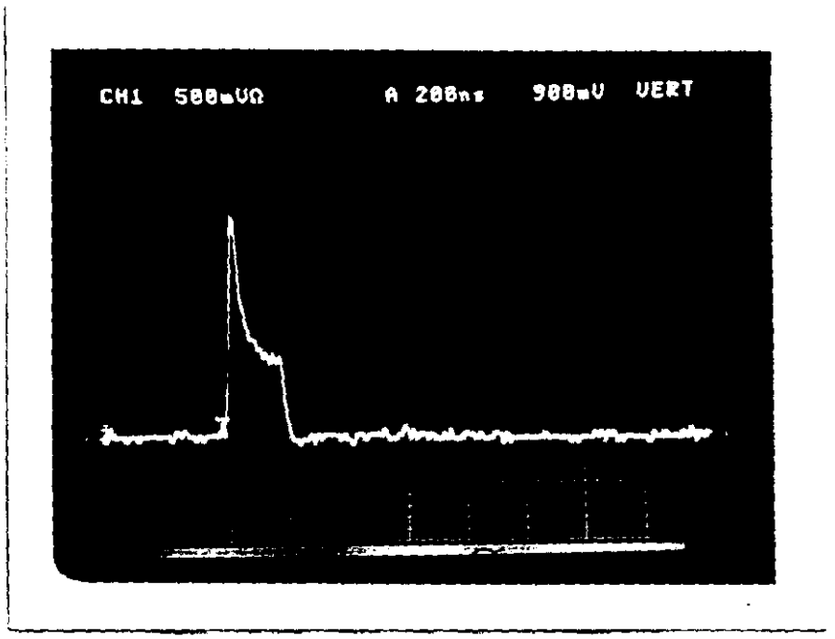

Fig 22 a

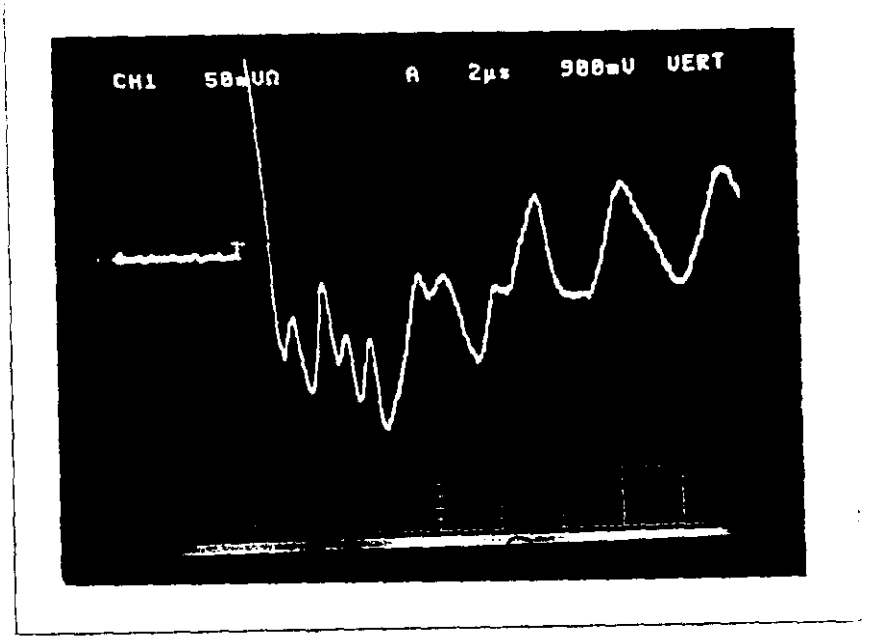

Fig 22c

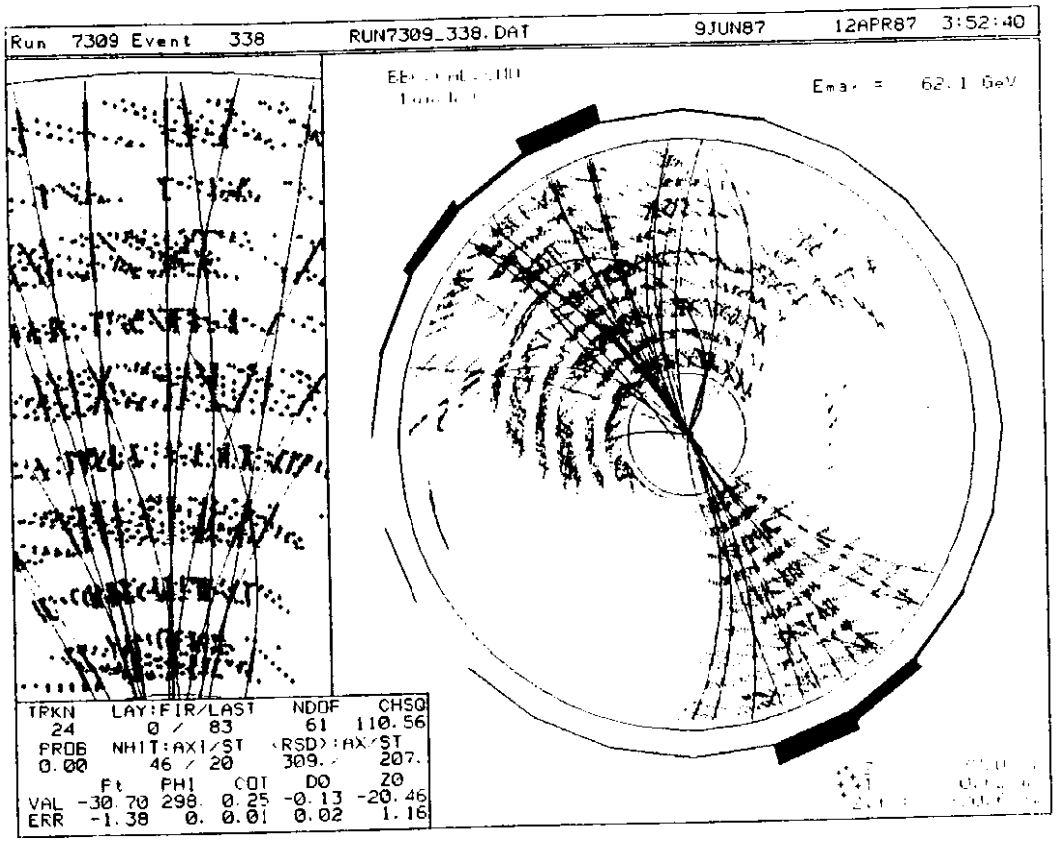
Run 7309 Event 338
RUN7309_338.DAT
9JUN87
12APR87 3:52:40
Emax = 62.1 GeV
TRKN LAY:FIR/LAST NDOF CHSQ
24 0 / 83 61 110.56
PROB NHIT:AXI/ST <RSD>:AX/ST
0.00 46 / 20 309. 207.
Ft PHI COT DO Z0
VAL -30.70 298. 0.25 -0.13 -20.46
ERR -1.38 0. 0.01 0.02 1.16

Fig 23

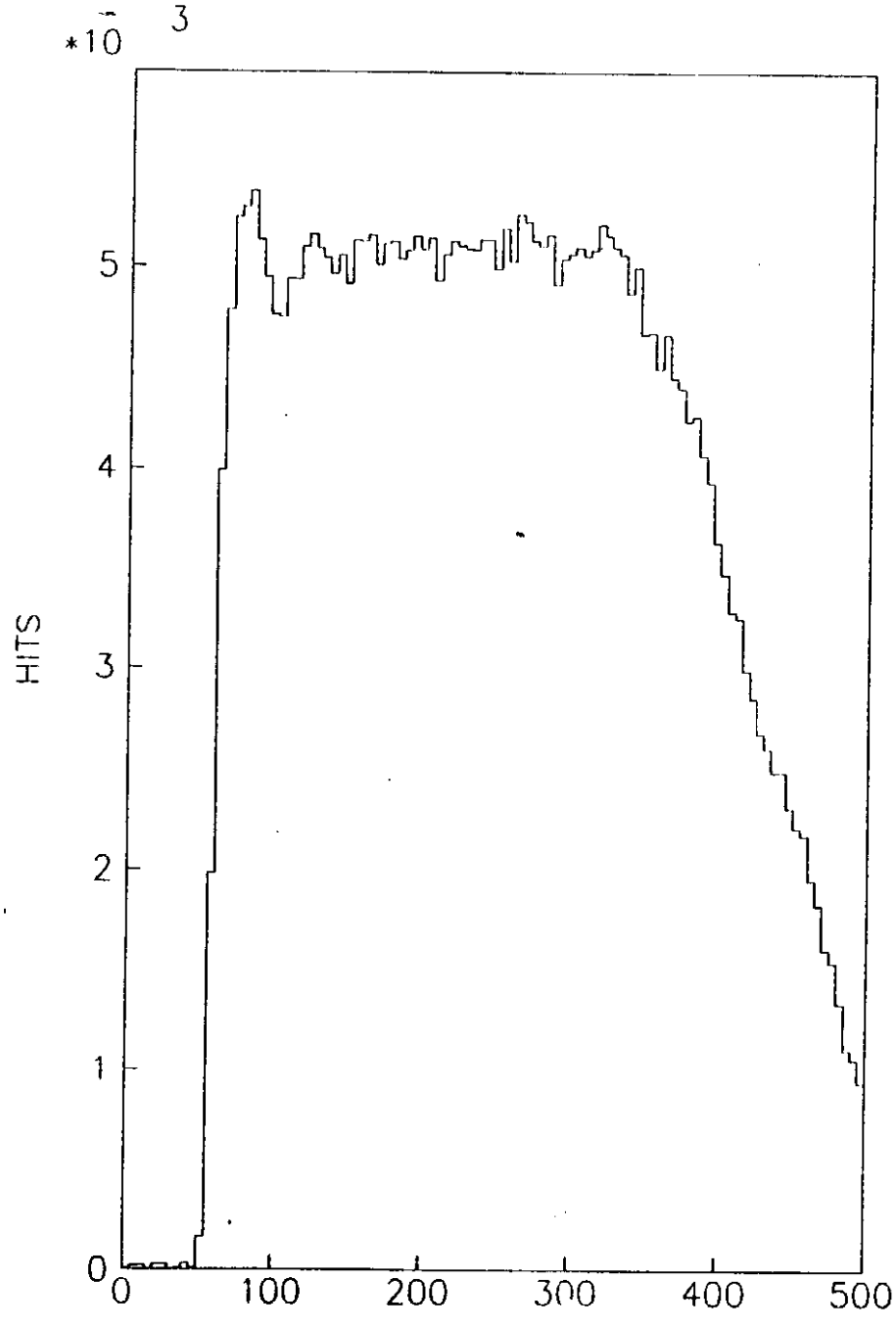

Fig 24

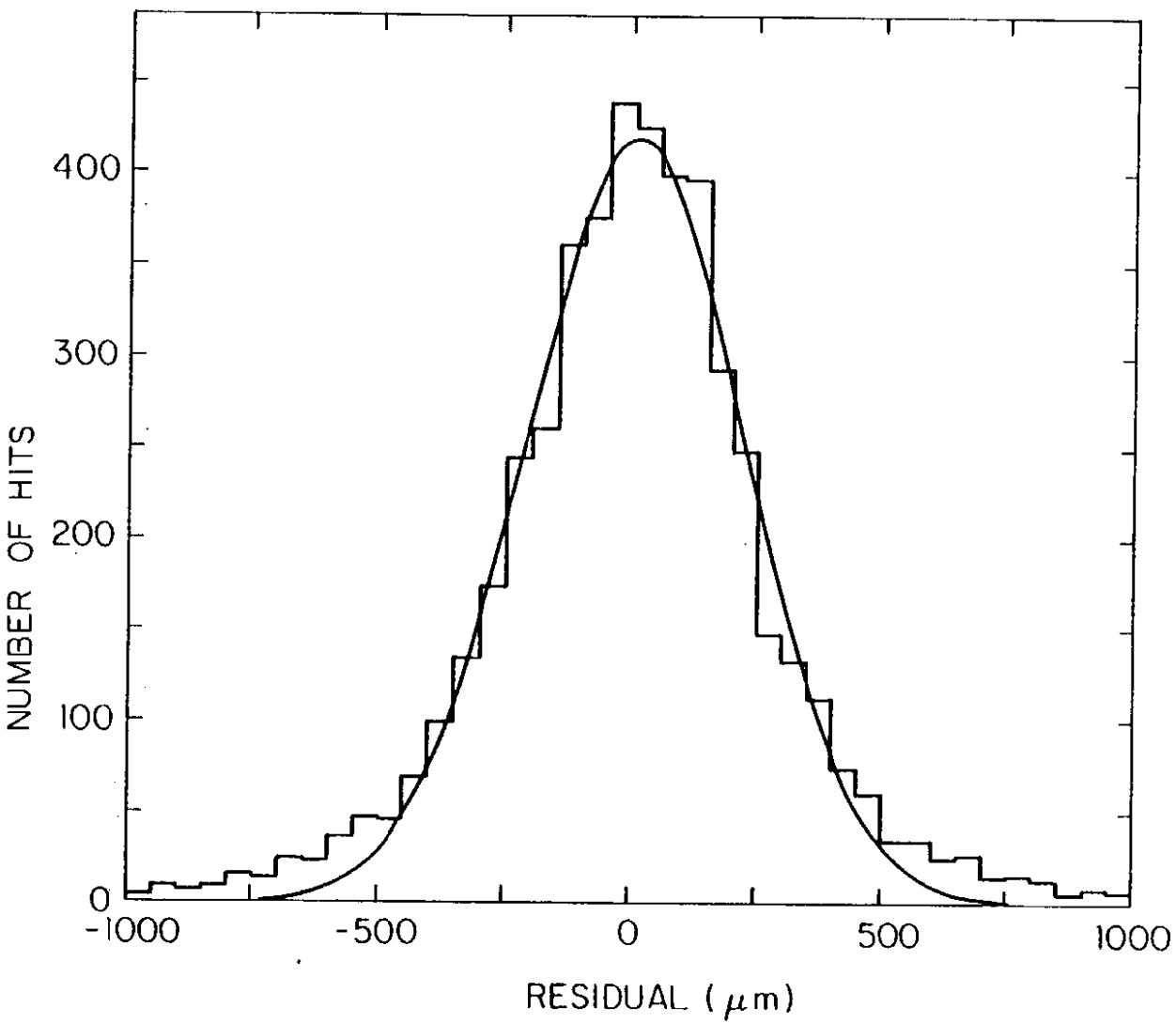
400
300
200
100
0
NUMBER OF HITS
-1000
-500
0
500
1000
RESIDUAL (μm)

Fig 25